Study on Electrical Power System combining centralized and distributed architectures to promote rapid development and survival improvement in Small Spacecraft

By

Jesus David Gonzalez Llorente

A thesis submitted for the degree of
Doctor of Philosophy in Engineering

Department of Applied Sciences for Integrated Systems Engineering
Graduate School of Engineering
Kyushu Institute of Technology
Japan

Kyutech
Kyushu Institute of Technology

Study on Electrical Power System combining centralized and distributed architectures to promote rapid development and survival improvement in Small Spacecraft

by Jesus David Gonzalez Llorente

A thesis submitted for the degree of Doctor of Philosophy in Engineering
Department of Applied Sciences for Integrated Systems Engineering
Graduate School of Engineering
Kyushu Institute of Technology, Japan

The doctoral dissertation supervisor and chair of doctoral dissertation approval committee:

Kei-Ichi Okuyama
Doctor of Engineering and Professional Engineer in Aerospace
Professor of Graduate School of Engineering,
Department of Space System Engineering,
Kyushu Institute of Technology.

The members of doctoral dissertation approval committee:

Mengu Cho, Professor
Department of Space Systems Engineering
Kyushu Institute of Technology
Tobata, Kitakyushu, Fukuoka, Japan

Koju Hiraki, Professor
Department of Space Systems Engineering
Kyushu Institute of Technology
Tobata, Kitakyushu, Fukuoka, Japan

Kazuhiro Toyoda, Associate Professor,
Department of Space Systems Engineering,
Kyushu Institute of Technology
Tobata, Kitakyushu, Fukuoka, Japan

Yasuhiro Akahoshi, Professor
Department of Space Systems Engineering,
Kyushu Institute of Technology
Tobata, Kitakyushu, Fukuoka, Japan

The committees have examined this dissertation and hereby certify that it is worthy of acceptance.

Kitakyushu, Fukuoka, Japan, 2019

Study on Electrical Power System combining centralized and distributed architectures to promote rapid development and survival improvement in Small Spacecraft

by

Jesus David Gonzalez Llorente

A thesis submitted for the degree of Doctor of Philosophy in Engineering

Abstract

Small spacecraft have been adopted by private companies and universities becoming more widespread in space applications. These programs do not have the same resources of traditional space programs; thus, low cost and fast delivery have been encouraged known as lean satellite programs. The delivery time of most of the small satellites is still more than two years and the failure rate of the small spacecraft is still a concern. Small satellites have the highest infant mortality rate and the Electrical Power System (EPS) is one the subsystems that contribute the most to the failure of CubeSats. To achieve fast delivery and low cost without compromise the reliability it is necessary to redefine the systems engineering of small spacecraft. Improvement in the development of EPS will contribute significantly to achieve the goals of low-cost and fast delivery of small spacecraft. The methods and guidelines for rapid development of electrical power systems have been proposed in this thesis. The architecture of EPS has been analyzed to diminish the failure rate that is related to the small spacecraft. In addition, a modular approach has been proposed to achieve rapid development and reliable systems. The module integrates the solar cells and the power condition units. Then, the EPS is designed integrating the required number of modules as it is demonstrated in Ten-Koh satellite.

Supervisor: Dr. Kei-Ichi Okuyama, Profesor of Department of Space System Engineering
Kyushu Institute of Technology

To my wife, Paula Andrea,

my source of happiness and motivation.

Thank you for being in every moment.

Acknowledgements

It would not have been possible to complete this thesis without the partnership of many people. First, I want to thank my supervisor Professor Kei-Ichi OKUYAMA. It has been a joy and a great privilege to work under his supervision during the development of my research. I want to thank him for providing me an enjoyable environment in his laboratory and all the necessary resources for the development of this thesis. Thanks for the opportunity to work in Ten-Koh satellite since formulation until operation as team leader of the Electrical Power System (EPS).

I also want to thank the members of my doctoral committee, Professor Mengu CHO, Koju HIRAKI, Kazuhiro TOYODA and Yasuhiro AKAHOSHI for his valuable comments and suggestion during the different reviews of this thesis. Their insightful questions and comments help me to clarify many points of this research. In addition, thanks to the professors and staff of the Space Engineering International Course (SEIC), the Graduate School of Engineering and Department of Applied Science for Integrated Systems Engineering.

This thesis would have not been possible without the collaboration of the members of Okuyama laboratory and the Ten-Koh development team. Special thanks to Aleksander A. Lidtke for his leadership to achieve Ten-Koh integration into a whole system and for his interest in this research on Electrical Power Systems. Our conversations while we were working in Ten-Koh satellite were very rewarding and enjoyable.

Special thanks to Ten-Koh Electrical Power System (EPS) team with whom I spent a lot of time working during the development of this system: Juan J. Rojas, Ken Hatanaka, Kiruki Cosmas, Thanks for their contribution and commitment during the development of the Ten-Koh EPS and the friendly environment during this endeavor.

In the same way, I am thankful to the members of Ten-Koh development team for his contributions to the development and operation of Ten-Koh satellite that allowed the data necessary for the validation of this research: Isai Fajardo, Rafael Rodriguez, Naoya Urakami, Misuzu Matsuoka, Ryo Kawauchi, Masayuki Miyazaki, Naofumi Yamagata, Farhan Abdullah, Limam Lakhdar, Rigoberto Morales, Sidi Ahmed Bendoukha, Dmytro Faizullin, Tuguldur Ulambayar and Mohamed Elhady Keshk.

I am thankful to the radio amateur community that was receiving the housekeeping data around the world. Special thanks to Scott(K4KDR), Rocco(W2RTV), Bob(N6RF1), Iji-san(JA6PL), Albert(PA5OXW), Otani-san(JH4DHX/3) and the SatNOGS community for the continuous support. Special thanks also to Adrian Sinclair (LU1CGB) and Matias Graio (LU9CBL) for receiving Ten-Koh signal for first time.

I am grateful to the Ministry of Education, Culture, Sports, Science and Technology of Japan (MEXT), the United Nations Office Outer Space Affairs (UNOOSA) and Kyushu Institute of Technology (Kyutech) for the financial support under the United Nations/Japan Long-term Fellowship Programme on Nano-Satellite Technologies (PNST) scholarship. I am thankful to the members of these organizations that made possible this programme.

This research was partially funded by the Oita prefecture government, Japan. Oita Prefecture Organization for Industry Creation. Working group for Ten-Koh development "Oita Challenger". Their support was fundamental to obtain the materials for this research during Ten-Koh development.

Finally, I want to acknowledge my wife, my parents and my brothers. I really appreciate all their sacrifices and patience. Their emotional support has been essential for the achievement of this goal.

Contents

Declaration ix

List of Figures xi

List of Tables xvi

Nomenclature xviii

1 Introduction 1

1.1 Motivation 1

1.2 Objectives 4

1.3 Thesis outline 4

1.4 Contributions 6

2 Analysis of EPS to improve mission assurance 7

2.1 Introduction 7

2.2 Approach of Architecture of Dual Bus Electrical Power System . . . 9

2.2.1 Single-bus Electrical Power System 10

2.2.2 Dual-Bus Electrical Power System 12

2.3 Comparison of Two Cases of Dual Bus Electrical Power System . . . 13

2.3.1 Spacecraft Description 13

2.3.2 Comparison of Architectures 14

2.4 Discussion of failure rate . . . 15
2.5 Summary . . . 19

3 Modular approach for power generation in EPS 20

3.1 Introduction . . . 20
3.2 A Modular Design Approach for Solar Array . . . 24
3.2.1 SMIC Architecture . . . 24
3.2.1.1 Solar Power Generation Unit . . . 26
3.2.1.2 Solar Array Regulator . . . 27
3.2.1.3 Telemetry Acquisition Unit . . . 27
3.2.2 SMIC Design . . . 28
3.2.2.1 Design of Solar Array Regulator . . . 28
3.2.2.2 Design of Solar Power Generation Unit . . . 29
3.2.3 SMIC Verification Approach . . . 31
3.3 Applying Solar Module Design to Ten-Koh Satellite . . . 34
3.3.1 Power Needs and Constraints for Case Study: Ten-Koh Satellite 34
3.3.1.1 Satellite Orbit . . . 35
3.3.1.2 Power Requirements . . . 35
3.3.2 Solar Array Regulator . . . 36
3.3.3 Solar Array Configuration . . . 37
3.3.4 Solar Module Measurements . . . 40
3.4 Experimental Results of SMIC . . . 41
3.4.1 Mechanical Qualification . . . 41
3.4.2 Thermal Vacuum Qualification . . . 45
3.4.3 Experimental Verification . . . 47
3.5 On-Orbit Results of Twelve SMIC . . . 50
3.6 Summary . . . 54

4 Results of EPS in small spacecrafts: Ten-Koh case 55

4.1 Introduction . . . 55

4.2 Power Source and Energy Storage 58
4.2.1 Solar Array 59
4.2.2 Batteries 59
4.3 Power Control Unit 60
4.3.1 Battey Charge and Discharge Control 60
4.3.2 Power deactivation switches 61
4.4 Power Regulation and Distribution 62
4.5 In-orbit results of Ten-Koh EPS 63
4.6 Summary 70

5 Experimental results of ultracapacitor in Low Earth Orbit on-board Ten-Koh 71

5.1 Introduction 71
5.2 Experiment 72
5.2.1 Supercapacitor selection 72
5.2.2 Design of experiment board 73
5.2.3 Experiment Integration in the spacecraft 75
5.2.4 Test during orbit operation 77
5.3 Results and discussion 77
5.3.1 Self discharge characterization 79

6 Conclusions 81

Bibliography 84

Declaration

The work in this thesis is based on research carried out at Okuyama Laboratory and it has been conducted as part of Ten-Koh satellite in the Department of Applied Science for Integrated Systems Engineering, Kyushu Institute of Technology, Japan. No part of this thesis has been submitted elsewhere for any other degree or qualification. This research has been conducted as part of the Space Engineering International Course.

Some of the work presented in this thesis has been already published in journals and conference proceedings - the relevant publications are listed below and they are properly referenced in the correspondent chapter:

Journals

- **Gonzalez-Llorente, J.**, Lidtke, A., Hurtado, R., & Okuyama, K. Single-bus and Dual-bus Architectures of Electrical Power Systems for Small Spacecraft. *Journal of Aerospace Technology and Management*. Vol. 11. October, 2019 https://doi.org/10.5028/jatm.v11.1086.

- **Gonzalez-Llorente, J.**; Lidtke, A.A.; Hatanaka, K.; Kawauchi, R.; & Okuyama, K. Solar Module Integrated Converters as Power Generator in Small Spacecrafts: Design and Verification Approach. *Aerospace* 2019, 6(5), 61. https://doi.org/10.3390/aerospace6050061

Conference Proceedings

- **Gonzalez-Llorente, J**., Okuyama, K., Fajardo Tapia, I., Szasz, B., Bendoukha, S., & Nishio, M. Evaluation of Orbit data of electrical power system of deep space probe Shinen2. In *Proceedings of 31th International Symposium on Space Technology and Science (ISTS)*. Matsuyama, Japan. June 3-9, 2017
- **Gonzalez-Llorente, J**., Rojas, J. J., Hatanaka, K., Fajardo Tapia, I., & Okuyama, K. (2019). On-Orbit result of electrical power system of LEO environment observation small satellite Ten-Koh. In *Proceedings of 32nd International Symposium on Space Technology and Science (ISTS)*. Fukui, Japan. June 15-21, 2019
- Fajardo Tapia, I., Bendoukha, S. A., Okuyama, K., Saganti, P., **Gonzalez-Llorente, J.**, Abdullah, F., & Lakhdar, L. Development of a set of instruments for a Small Satellite mission to observe the LEO environment in the presence of a decreasing solar cycle. In *Proceedings of 32nd International Symposium on Space Technology and Science (ISTS)*. Fukui, Japan. June 15-21, 2019

List of Figures

1.1 Delivery time of small satellite. Source [1] 2
1.2 Failure of University-Class missions. Source: [2] 3
1.3 Contribution of each subsystems to the failure of Cubesat after 30 days since ejection. Source: [3] 3

2.1 (a) Architecture of simple electrical power system on a small spacecraft and its interfaces with other subsystems. (b) Block diagram of a PCM indicating functional components 9
2.2 Probability of failure and cost versus the number of units in parallel. Decrease of probability of failure for units placed in parallel is minimum for more than three units, however cost of is increasing significantly . . 11
2.3 (a) Architecture of single bus electrical power system with duplicated EPS. (b) A failure in EPS 1 will prevent the operation of PL-1 and ADCS indicated by the red marks in the figures. EPS 2 can be designed to support essential elements for minimum satellite success i.e. OBC, COM and PL-2. 12
2.4 (a) Architecture of dual bus electrical power system with duplicate components. (b) A failure, indicated by the red marks, in EPS 1 will cause the loss of OBC-1, COM-1, ADCS-1 and PL-1. However, COM-2, OBC-2 and PL-2 can still operate receiving the power from EPS 2. 13

2.5 Example of two small spacecrafts with body mounted solar arrays (a) Nanosatelite following the three unit CubeSat dimensions (b) Micro deep space probe Shinen-2. 14
2.6 Electrical power system architecture of micro deep space probe Shinen-2 15
2.7 Power distribution of nanosatellite. EPS 2 has enough installed capacity to only power the OBC and COM-2 subsystems, while EPS 1 can power all subsystems. Hot redundancy is used selecting DC-DC converters that support parallel connection 16
2.8 Schematic representations of the two components A and B arranged in architectures with varying levels of redundancy. a) Dual redundant power system. b) Fully redundant (cross-strapped) power system. c) Single string system 17
2.9 Failure probability comparison assuming all the components has the same value 18

3.1 Solar Module Integrated Converter applied to Ten-Koh satellite: external view with solar cells and internal view where PCB with solar array regulator is shown. 24
3.2 Architecture of EPS with multi-array of solar cells using Solar Module Integrated Converter (SMIC). 25
3.3 Architecture of Solar Module Integrated Converter (SMIC). 25
3.4 The sequence of qualification tests proposed to the SMIC. In the sequence of the tests on the left, solar arrays are not included in the tests to reduce the risk of damaging the expensive solar cells. Only the TMA and SAR units of the SMIC are tested there, shown in green. Solar arrays are tested in the sequence on the right, with PV curves obtained at the purple steps in the process. The complete SMIC was functionally tested with the battery at the end of the qualification process, shown in red. 33

3.5 Two orientation scenarios of Ten-Koh satellite: (**Left**) worst-case scenario for power generation because the least area is exposed to solar radiation; and (**Right**) best case for power generation. The launcher adapter ring is shown in yellow. 39
3.6 The sequence of mechanical tests conducted on the qualification model of the solar panel. The same sequence also applies to the satellite EQM test, but modal survey was carried out after each test during the satellite system-level tests. 42
3.7 Power spectral density applied to the SMIC. Showing the natural frequency of the solar array derived using finite-element modelling (315 Hz) with a black line. $|PSD|$ shown in red, PSDs measured along individual SMIC axes in other colors. 45
3.8 SMIC setup in Ten-Koh STM during vibration. 45
3.9 Temperature and pressure during TVAC qualification of solar module. . 46
3.10 Temperatures measured by thermocouples located on the unit obtained during TVAC qualification of SMIC. The pressure in the chamber throughout the test, which was always lower that 1.0×10^{-4} Pa, is also shown. . 47
3.11 SMIC in the sun simulator. 48
3.12 Experimental power–voltage (P-V) curve of one solar cell of the module. 48
3.13 Evaluation of MPPT performance by comparison the power obtained and the maximum available power. 49
3.14 Time series of the battery voltage and the charge currents of both Ten-Koh batteries recorded since the launch. The LOWESS regression through the time series is also shown. Negative current has been defined to be charging the battery. 51

3.15 Histogram of the charge currents of both Ten-Koh batteries recorded since the launch. The sum of the two currents, and their mean and median are also shown. Negative current has been defined to be charging the battery. Y-axis reports the fraction of all measurements that saw a current greater than the corresponding X-axis value. 52
3.16 Battery voltage (V_{BAT}), battery current (I_{BAT}) and total generated power by the SMICs (P_{SMIC}) during one orbit. 53
3.17 Time series of the difference between currents of batteries 1 and 2 ($\Delta I_{BAT} = I_{BAT1} - I_{BAT2}$) during one orbit. Negative current has been defined to be charging the battery. 54

4.1 Flight model of Ten-Koh satellite. 56
4.2 Architecture of Ten-Koh EPS 57
4.3 Inhibit schematic 62
4.4 Power distribution in ADS systems 63
4.5 Power distribution in DLP systems 64
4.6 Ten-Koh CAD view. External view with solar panels (left). Internal view showing the battery 1, battery is located in the opposite side and it is not shown (right) 65
4.7 Ten-Koh external and internal view 66
4.8 Ten-Koh first orbit identified as 2018-084G 68
4.9 History of battery voltage since launching 68
4.10 History of battery currents since launching 69
4.11 History of battery temperature since launching 70

5.1 Components of the charger and discharger experiment 73
5.2 Implemented experiment board 74
5.3 Location of UCP experiment board in the spacecraft in the CAD model. 76
5.4 Location of UCP experiment board in the spacecraft in the Flight model. 76
5.5 One cycle charging and discharging the UCP. 78

5.6 Voltage and current during charging and discharging the UCP. 79
5.7 Temperature during charging and discharging the UCP. 79

List of Tables

3.1 Power consumption of Ten-Koh subsystems. 36

3.2 Maximum electrical ratings of the selected MPPT. 37

3.3 Parameters of triple junction cells for cells of 26.5 cm^2 and 30.15 cm^2 for standard conditions (1367 W/m^2, 28 °C). 38

3.4 Comparison of the number of cells for three design approaches: maximum area approach vs. modular approach with area analysis and power balance. 39

3.5 Mechanical qualification test conditions used to test the SMIC. X refers to the satellite longitudinal (aligned with the launch vehicle acceleration) axis, while Y and Z axes complete the orthogonal triad. 43

3.6 Durations of hot and cold dwells during Thermal vacuum cycles. 47

3.7 Measurement during test of SAR as MPPT. 50

4.1 Parameters of Ten-Koh initial orbit 56

4.2 Power consumption of Ten-Koh subsystems. 57

4.3 Electric specification of Solar cell at AM0 (1367 W/m^2), 25° C. 59

4.4 Specification of Lithium-Ion battery cell NCR18650B 60

4.5 Electric specification of battery charge with MPPT SPV1040 61

4.6 Specification of battery protection circuit S-8261 61

4.7 Inhibit scheme 62

4.8 Ten-Koh housekeeping during first orbit 67

5.1 Specifications of the supercapacitor 73

5.2 UCP self-discharge calculation 80

Nomenclature

AO adaptive optics

SMIC Solar Module Integrated Converters

EPS Electrical Power System

LEO Low Earth Orbit

SAR Solar Array Regulator

MPPT Maximum Power Point Tracking

DET Direct Energy Transfer

I2C Inter Integrated Circuit

SPI Serial Peripheral Interface

TMA Telemetry Acquisition

COTS commercial Off-The-Shelf)

QM Qualification Model

PFM Proto-Flight Model

FEM Finite Element Model

OBC On-Board Computer

COM Communication Subsystem

ADS Attitude Determination Subsystem

ECU Experiment Control Unit

DLP Double Langmuir Probe

CPD Charge Particle Detector

ADC Analog to Digital Converter

EQM Engineering Qualification Model

S/C Spacecraft

PSD Power Spectral Density

TVAC Thermal Vacuum

STR Structure

DE Deployment

Chapter 1

Introduction

Nowadays the number of small satellites have increased drastically. This has been possible due to the participation of new space actors such as private companies and universities [4]. This is not a role of government and military's anymore. Small satellites are not new systems, they have been from beginning of the space era. However, Small spacecraft are key elements in space applications such as technology demonstrations, education and science. In this chapter, the reasons to study Electrical Power Systems in small spacecraft are discussed looking recent statistics about the delivery time and the failure of university-class missions. In addition, the goal and contributions of this research are summarized and the thesis outline is presented.

1.1 Motivation

Traditional satellite development philosophy cannot be applied to small spacecraft because the new developers do not have the same resources. Thus, the application of lean satellite program has been encouraged to promote the space sector because this program emphasizes low-cost and fast delivery approach [5]. When the deliver time of small satellites is reviewed [1], it has been found that only 41% of the satellites has a deliver time of less than two years (Fig. 1.1).

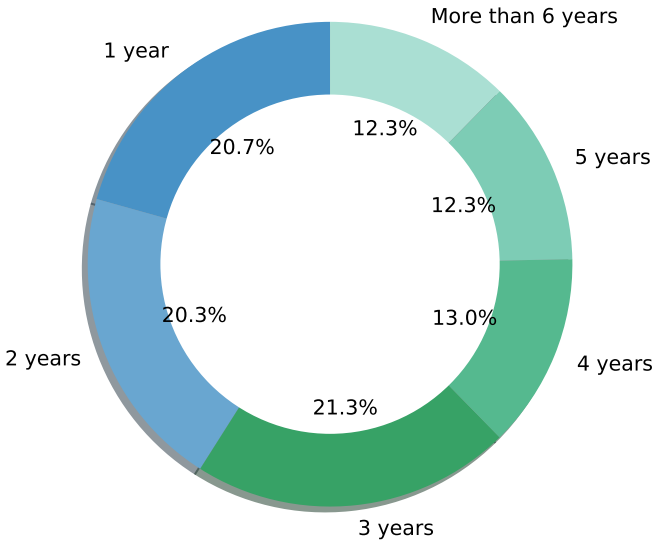

Figure 1.1: Delivery time of small satellite. Source [1]

This approach has contributed to the proliferation of small spacecraft in recent years. The number of small satellites has increased significantly. However, the failure rate of the small spacecraft is still a concern. Small satellites have the highest infant mortality rate. According to the review of university-class mission, less than 50% of the missions achieve partial or full mission success [2]. Without considering the launch fail, this review shows that 39% of university-class mission do not achieve the minimum mission success (Fig. 1.2).]

The causes of satellite failure has been related to the different spacecraft subsystems [3]. Thus, the EPS has been identified as the main cause of failure in CubeSats after 30 days of operation (Fig. 1.3). Therefore, if the failure rate of the EPS is decreased then the failure rate of the spacecraft is also decresed.

Even though the lean approach has been adopted, systems engineering for small spacecraft, that combines all the body of knowledge, has not been redefined yet to coverage the need of low-cost and fast delivery. Some progress has been achieved as the release of the test methods and test requirements in ISO standard 19683:2017 [6]. Additionally, the Definition and Requirements of Small Satellites Seeking Low-Cost and Fast Delivery have also been published. Despite this progress, there is not

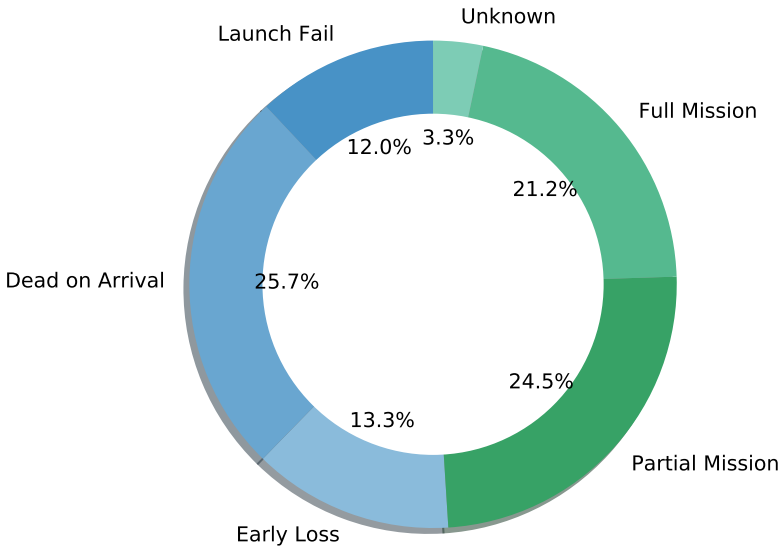

Figure 1.2: Failure of University-Class missions. Source: [2]

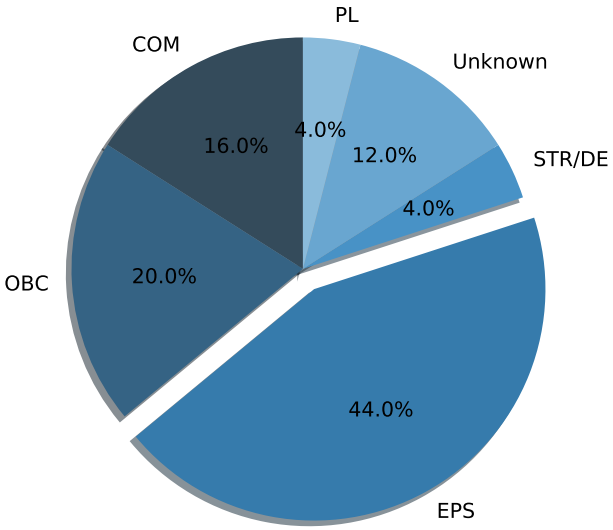

Figure 1.3: Contribution of each subsystems to the failure of Cubesat after 30 days since ejection. Source: [3]

enough guidelines, methods for the design of the spacecraft systems that facilitate the low-cost and fast delivery [7].

1.2 Objectives

This research aims to contribute with new methodologies and concepts for the development of small spacecrafts following the lean satellite philosophy. Specifically, the contributions are in the electrical power systems because the Electrical Power Systems (EPS) is transverse to all the spacecraft systems. In addition, the EPS is one of the spacecraft subsystems with highest failure rate and one of the most critical systems for the mission success. Thus, improvement in the development of EPS will contribute significantly to achieve the goals of low-cost and fast delivery of small spacecraft. The specific objectives of this research are the following.

- Evaluate the EPS architecture to improve the probability of mission success
- Develop a method of EPS development for fast delivery and low cost

1.3 Thesis outline

The methods and guidelines for rapid development of electrical power systems have been proposed in this thesis. The architecture of EPS has been analyzed to diminish the failure rate that is related with the small spacecraft. In this way the minimum success shall be achieved to assure the sustainability of the space programs.

In Chapter 2, the architecture of EPS has been analyzed to diminish the failure rate that is related with the small spacecraft. In this way the minimum success shall be achieved to assure the sustainability of the space programs. An analysis of a Single-bus and Dual-bus Architectures is presented. The advantages of these architectures are discussed in the context of mass, efficiency, and failure rate. This

chapter uses material from reference [8] that corresponds to first journal publication on this thesis.

In Chapter 3, a modular approach has been proposed to achieve rapid development and reliable systems. One module, called Solar Module Integrated Converter, that integrates the solar cells and the power condition units have been proposed. Then, the EPS is designed integrating the required number of modules. It is very difficult to have a unique design that can meet the requirement of all satellites, then, the guidelines for designing the modules have been proposed and described. This chapter incorporates the reference [9], which is the second publication derived of this thesis.

In Chapter 4, a hybrid EPS that combines centralized and distributed architecture to take advantages of the Solar Module Integrated Converter is described. The EPS has been designed for Ten-Koh satellite. This chapter presents the architecture and main components an it also analyzes the in-orbit results of the designed EPS as well as the results of the ultracapacitor demonstration as secondary energy storage device in Low Earth Orbit (LEO).

In Chapter 5, the design a flight experiment to demonstrate the application of ultracapacitor in space. The results demonstrate that ultracapacitor can survive to the launch environment, charging and discharging of supercapacitor in LEO orbit is possible. And, self-discharge measurements after 1500 LEO orbits for different temperature and time is also presented.

In Chapter 6, the summary and conclusions are presented. The EPS architecture that was proposed and evaluated in Ten-Koh satellite can serve as guidance for future space missions that require the development of small spacecrafts. In the same way the design considerations and the concepts and methods presented can be a step forward for the small satellites' community.

1.4 Contributions

It was shown, based on the two satellite examples, that using a dual-power bus can offer increased reliability at a modest increase in mass, volume and complexity, which is also proportional to development risk. Therefore, it is recommended to evaluate the dual-bus power architecture when choosing the EPS architecture for small satellites.

Using SMIC for solar power generation reduces the complexity in both design and testing for small satellites. This effectively reduces the development time and costs of the mission without sacrificing quality and reliability because only one module is designed and qualified to confirm that it meets the functional requirements, as well as it withstands the launch and in-orbit environments. Then the required number of SMIC are manufactured.

A redundant EPS was developed for quasi-spherical satellite in LEO, Ten-Koh. The designed architecture included the proposed SMIC, allowing the validation of redundancy in a solar multi-array that uses 12 identical modules. The received housekeeping data since launching date confirmed the validation and verification of the proposed EPS.

This thesis designed an experiment to demonstrated the application of ultracapacitor in LEO. The results have demonstrated that the COTS supercapacitor evaluated withstood the LEO environment conditions and the launching environment without thermal o mechanical protection.

Chapter 2

Analysis of EPS to improve mission assurance[†]

The development of spacecraft by universities has increased recently with the launching of nanosatellites, picosatellites and miniaturised deep space probes. However, there is still a high probability of failure and many small satellites do not achieve minimum mission success. Considering that EPS is one of the main contributor of failure, it is necessary to study how to improve the mission success by reducing the failure rate of EPS. This chapter discusses different ways of redundancy that can be used in small spacecraft[8].

2.1 Introduction

Most of the university-class missions have adhered to the CubeSat specification to easily obtain a launch opportunity and used Commercial Off-The-Shelf (COTS) components to shorten the development time [10]. The popularity of university-built CubeSats can be demonstrated by reviewing the number of university missions that have already launched; 266 university-class missions had launched until the

[†]This chapter is based on the first publication of this thesis: 'Single-bus and Dual-bus Architectures of Electrical Power Systems for Small Spacecraft' by **Gonzalez-Llorente, J.**, Lidtke, A., Hurtado, R., & Okuyama, K. *Journal of Aerospace Technology and Management*. Vol. 11. October, 2019, available at https://doi.org/10.5028/jatm.v11.1086 under a Creative Commons Attribution license CC BY 4.0

end of 2015 [2]. Moreover, a new business based on a constellation of CubeSats conducting Earth observation is in operation [11]. Similarly, interplanetary and deep-space exploration missions have also been developed by universities [12–14]. One implicit goal of CubeSat development is having fast and low-cost projects; however, a high probability of failure is a common drawback associated with these projects. The failure rate of university-class missions is about 40% [2]; the electrical power system (EPS) is one of the main causes of failures of CubeSat missions both in early mission phase and during the first three months [3]. Thus, improving the reliability of the EPS will significantly reduce the failure rate of these missions. In small satellites, simple configurations have predominantly been used for implementing the electrical power systems [15, 16]. The power source (PS) of small satellites is typically based on solar cells, and lithium batteries as a secondary source [17]. The electrical power is transferred from the solar cells to the batteries and the spacecraft subsystems using either Maximum Power Point Tracking (MPPT) or Direct Energy Transfer (DET) architectures [18, 19]. In any case, a battery charge regulator (BCR) is required to protect the battery against overvoltage or overcurrent, and power conditioning modules (PCM) are needed to regulate and distribute the voltage for satellite subsystems. Fig. 1a shows the architecture of a simple EPS, showing its interfaces with main subsystems of the spacecraft: On-board Computer (OBC), Communication System (COM), Attitude Determination and Control System (ADCS) and Payload (PL). Fig. 2.1 shows the block diagram of main components of a PCM.

Placing two identical components in parallel significantly increases the reliability of a system, reduces the operating stress on the components and prolongs their expected life [18]. Splitting the power conditioning unit has been studied in high-power spacecraft to ease thermal control and to double the output power capacity [20]. In this chapter, two configurations with dual electrical power systems are presented. These configurations have been developed for a nanosatellite and a micro deep-space probe, Shinen-2 [21], which was launched in December 2014 on-board

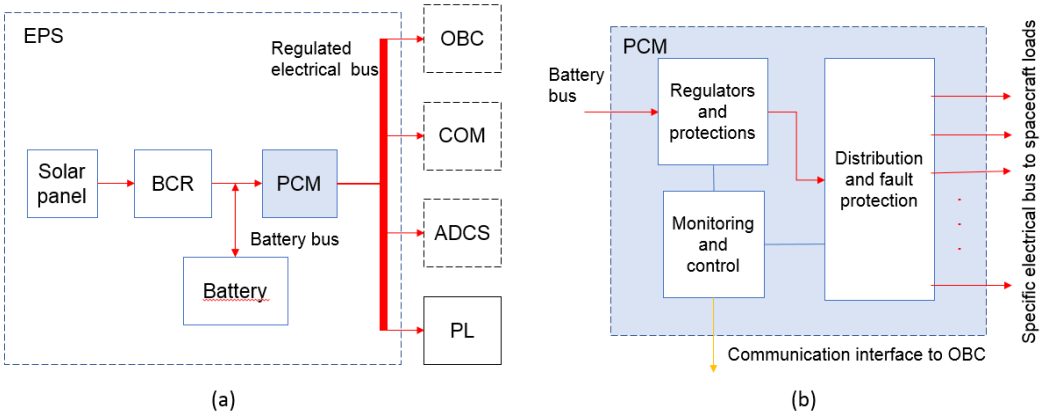

Figure 2.1: (a) Architecture of simple electrical power system on a small spacecraft and its interfaces with other subsystems. (b) Block diagram of a PCM indicating functional components

H-IIA-202. The next section of the chapter presents the general approach to the implementation of the dual bus electrical power systems for two cases. Then, a detailed comparison of the two case studies for a nanosatellite and deep-space probe is made. Because the two missions have different needs, this comparison is focused on showing the performance of different units used in the implementation of the EPS, not the overall systems. The objective is to provide reference designs of the EPS functional units for future spacecraft. The results section shows measurements of the performance of the two case studies including on-orbit data from the deep-space probe, and the theoretical failure rate is discussed. Finally, conclusions regarding the merits of a dual-bus EPS architecture in the context of small satellites are drawn.

2.2 Approach of Architecture of Dual Bus Electrical Power System

Most of the spacecraft are designed to achieve specific missions performing different functions in science, technology demonstration or education. For university-class spacecraft, receiving the housekeeping data of the satellite is usually considered minimum success of the mission because one of the primary objectives is education.

It is thus considered sufficient for the the team, formed mainly of students, to be able to develop a functional spacecraft. In cases with multiple mission objectives, it is usual to consider multiple reliability requirements; achieving any of these requirements is a level of the mission success [22]. For example, in the hypothetical case of one spacecraft with two missions and two payloads (PL-1 and PL-2), the mission requirements could include the following:

- At least PL-1 shall be operational for minimum success of mission 1,
- At least PL-2 shall be operational for minimum success of mission 2,
- Both PL-1 and PL-2 shall be operational for full mission success.

Usually, including more components needed to satisfy the minimum success is a common way to increasing the reliability of the mission. However, more components usually increase the cost and development time. As figure of merit (FOM), probability of failure (given by 1 - reliability) and cost of units in parallel can be used as trade-off criteria when designing an architecture with redundancy. The theoretical relationship between these two FOMs, that does not account for e.g. cost reduction with mass production, is shown in Fig. 2.2. It can be seen that the highest increase in reliability (or the highest decrease of probability of failure) is achieved with two components in parallel and the cost is increased linearly with the number of units [18]. Thus, two EPS designs approach are presented below: single-bus electrical with two units and two units in a dual bus; adding subsequent buses would follow the law of diminishing returns but would be associated with substantial increases in cost and complexity.

2.2.1 Single-bus Electrical Power System

A generalised architecture of the considered single bus EPS is shown in Fig. 2.3. The architecture is split into two systems, EPS 1 and EPS 2. Each EPS consists of a power source (PS), Battery, BCR and PCM. In a simple case, both systems have

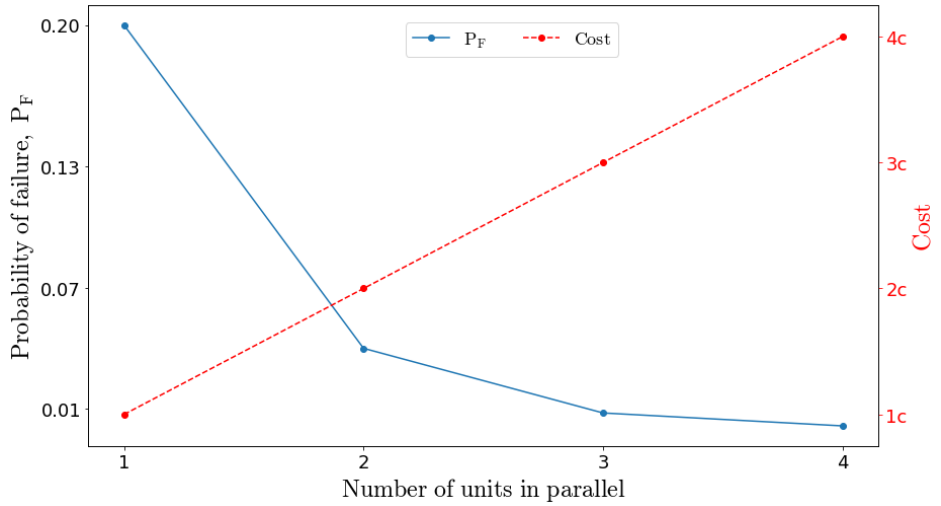

Figure 2.2: Probability of failure and cost versus the number of units in parallel. Decrease of probability of failure for units placed in parallel is minimum for more than three units, however cost of is increasing significantly

the same power capability and can provide the power required for all operation modes of the spacecraft. However, this case might be unattractive due to the mass and dimensional penalties implied by duplicating every component. One variation of the redundant architecture is to size the power sources of EPS 2 for operation of only the essential elements needed to achieve the minimum success of the mission (Fig. 2.3). For example, only OBC, COM and payload 2 (PL-2) may need to be powered from this bus; it means that ADCS is only essential element for mission of payload (PL-1).

In the case where EPS 2 only needs to provide power for selected subsystems, the number of solar cells and battery capacity are calculated accordingly to the power profile of these subsystems. The capacity of battery-2 in Wh ($E_{Battery2}$) is calculated by

$$E_{Battery2} = \frac{P_{OBC} \cdot T_{OBC} + P_{COM} \cdot T_{COM} + P_{PL1} \cdot T_{PL1}}{DOD_{Battery2} \cdot \eta_2} \tag{2.1}$$

where P_{OBC}, P_{COM}, P_{PL1}, T_{OBC}, T_{COM}, T_{PL1} are the power and time required for OBC, COM and PL1 during eclipse; $DOD_{Battery2}$ is the depth of discharge for

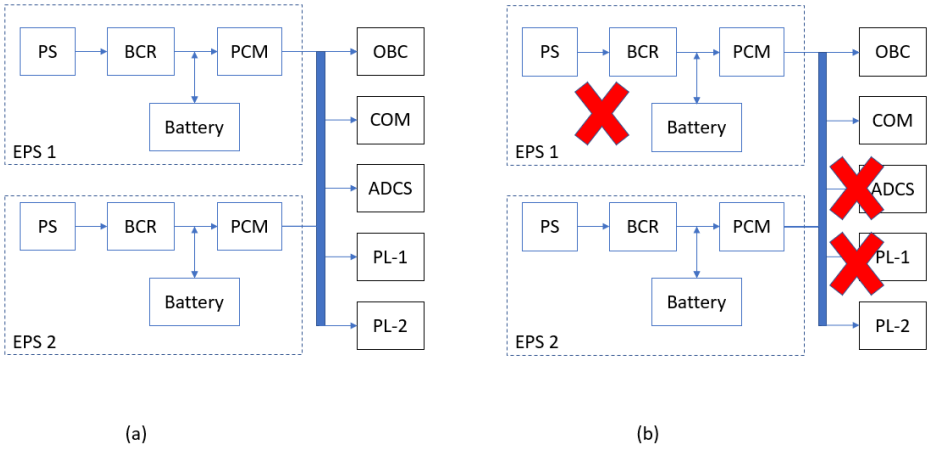

Figure 2.3: (a) Architecture of single bus electrical power system with duplicated EPS. (b) A failure in EPS 1 will prevent the operation of PL-1 and ADCS indicated by the red marks in the figures. EPS 2 can be designed to support essential elements for minimum satellite success i.e. OBC, COM and PL-2.

battery 2 and η_2 is the efficiency of the charge/discharge modules.

2.2.2 Dual-Bus Electrical Power System

The spacecraft can include redundancy of subsystems different to the EPS such as OBC and COM to increase the probability of mission success. These additional subsystems are not necessarily identical to avoid the same errors when executing the same operation, e.g. two communication subsystems might use different frequency bands [23]. The dual bus architecture for this case can be implemented as shown in Fig. 2.4. Here, the two power buses are separated, thus, EPS 2 provides power just to the communication (COM-2), the controller unit (OBC-2) and the secondary payload (PL-2).

The main reason to include dual electrical power systems is to reduce the failure rate of the whole spacecraft. Thus, the spacecraft should be able to operate when one of the power systems fails. This is the case for the micro deep-space probe Shinen-2, where the dual bus is implemented: one bus provides power to the sensing payload (radiation particle detector) and one communication subsystem, while the other bus provides power to another communication subsystem that is sufficient for up-

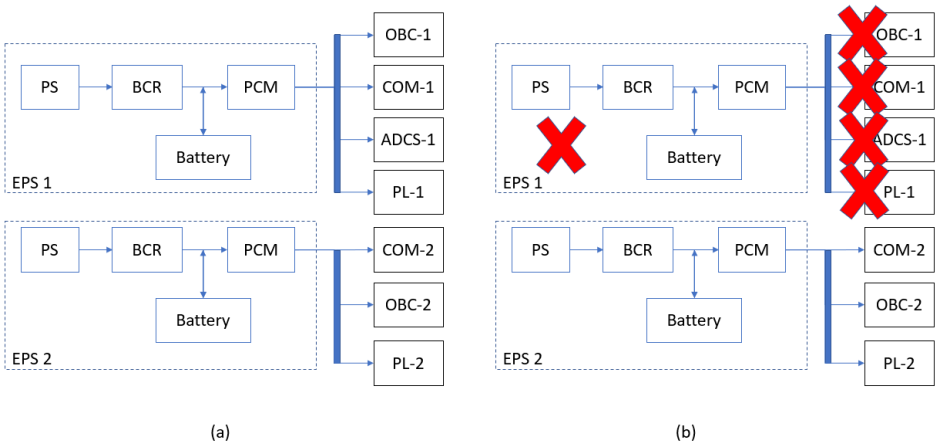

Figure 2.4: (a) Architecture of dual bus electrical power system with duplicate components. (b) A failure, indicated by the red marks, in EPS 1 will cause the loss of OBC-1, COM-1, ADCS-1 and PL-1. However, COM-2, OBC-2 and PL-2 can still operate receiving the power from EPS 2.

and down-link on its own. Different approach is implemented in the nanosatellite. It is not made fully redundant because the secondary power system can only provide power for minimum operating conditions. Namely, OBC and COM have backup power lines from a separate power source. These two power systems will be analysed in next section.

2.3 Comparison of Two Cases of Dual Bus Electrical Power System

2.3.1 Spacecraft Description

The nanosatellite taken as an example here is a three-unit (3U) CubeSat, dimensions of which are 30 by 10 by 10 cm and the mass is 4 kg (Fig. 5a). The main mission is to take a photograph of the Earth using a camera developed with COTS components. Moreover, this is a university-class mission that involves students in the development team as part of education and research projects.

The exemplar micro deep-space probe, Shinen-2, has a quasi-spherical shape, dia-

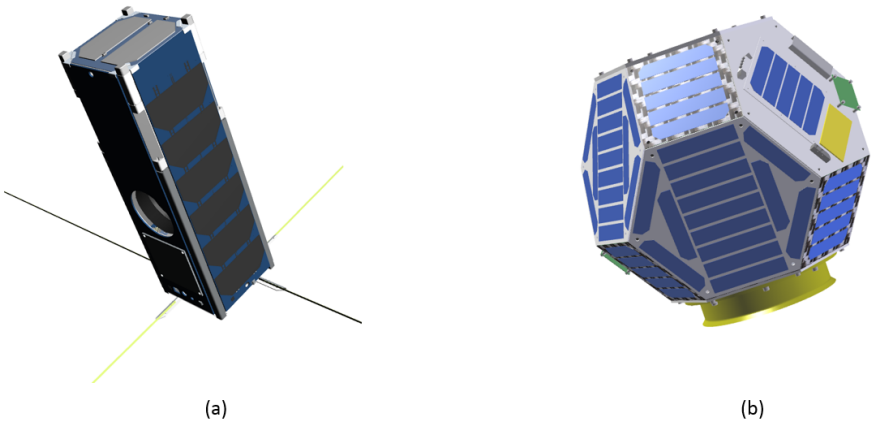

Figure 2.5: Example of two small spacecrafts with body mounted solar arrays (a) Nanosatelite following the three unit CubeSat dimensions (b) Micro deep space probe Shinen-2.

meter of about 50 cm and mass of 18 kg (Fig. 5b). This probe was developed with three purposes: firstly, to demonstrate a structure based on Carbon Fiber Reinforced Thermoplastic (CFRTP); secondly, to measure radiation from Earth to deep space with a charge particle detector, and thirdly, to demonstrate a deep space communication method [24].

2.3.2 Comparison of Architectures

The electrical power system of Shinen-2 uses a dual-bus system with duplicate components as described in the previous section. A block diagram of the dual electrical power system of Shinen-2 is shown in Fig. 2.6. This redundant system aims to have an independent power line for each communication line. Thus, EPS 1 provides power to the main communication line (COM-1) that include the beacon transmitter (TX-Beacon), the OBC-1 and the main payload (PL-1). The EPS 2 provides power to the deep-space communication (COM-2) that is itself a technology demonstration payload (PL-2). Both power systems include Solar Array Panels (SAPs) as power source (PS), Maximum Power Point Tracking (MPPT) as BCR, Power Conditioning Module (PCM) and protections.

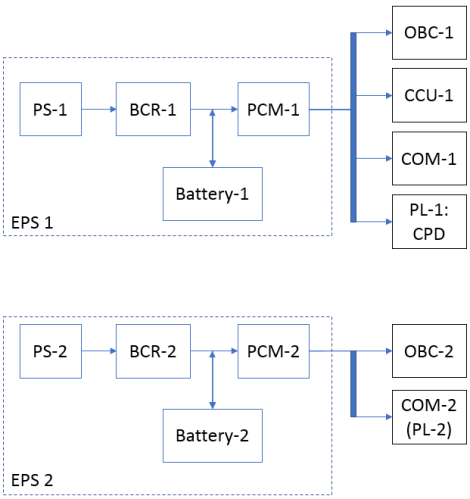

Figure 2.6: Electrical power system architecture of micro deep space probe Shinen-2

Instead of using the dual-bus power system, the electrical power system of the nanosatellite uses a single bus electrical power system. However, the components of EPS 2 are sized for minimum operation condition (OBC and COM-1) as described in previous section, and EPS 1 is sized for full operation (OBC, COM-1, COM-2, ADCS and PL). EPS 2 is called secondary power system and provides less power than the solar arrays used in the EPS 1 (main power system). The operating modes that rely on the secondary power system are designed to use only the essential subsystems and have a positive power budget. A block diagram of the EPS of the nanosatellite is shown in Fig. 2.7, and the description of each component is presented in the following section. Implementation of hot redundancy can be used by careful selection of DC-DC converters that achieve stable voltage regulation and load sharing when operated in a parallel connection [25].

2.4 Discussion of failure rate

The nanosatellite and the deep-space probe use single and dual-bus power systems, respectively. These are variations of the simplest possible architecture of an electrical power system with no redundancy. This section presents an analysis of these architectures focused on the failure probability.

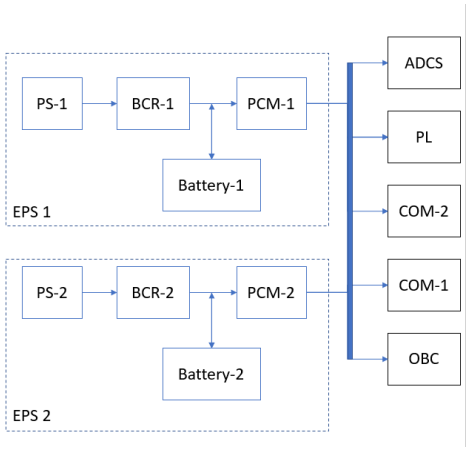

Figure 2.7: Power distribution of nanosatellite. EPS 2 has enough installed capacity to only power the OBC and COM-2 subsystems, while EPS 1 can power all subsystems. Hot redundancy is used selecting DC-DC converters that support parallel connection

Given components A and B, e.g. overcurrent protection and regulation ICs, each with a failure probability P_A and P_B, different arrangements of these components will result in different failure probabilities of the complete A-B assembly, P_F. Note that the analysis presented here applies directly to the EPS architectures presented before, even though the actual equations may need to be written for more than only two components. Limiting the analysis to only two components makes the results more succinct, and is therefore favoured over an in-depth failure probability analysis of the presented exemplar EPS architectures.

Different ways in which components A and B can be arranged are schematically shown in Fig. 2.8. For the sake of clarity, only dual redundancy is shown, even though more than two components could be placed in parallel to further reduce P_F. Also note that P_F analysed here is the probability of failure, i.e. the complement of reliability. For the simplest, single string arrangement from Fig. 2.8c, the failure probability is the highest of the three presented in Fig. 2.8 [26]:

$$P_{F,C} = P(A \cup B) = PA + PB - PA.PB \tag{2.2}$$

However, such a system is the least complicated and thus the quickest to test and implement. Moreover, it requires the least PCB space, which might be an important

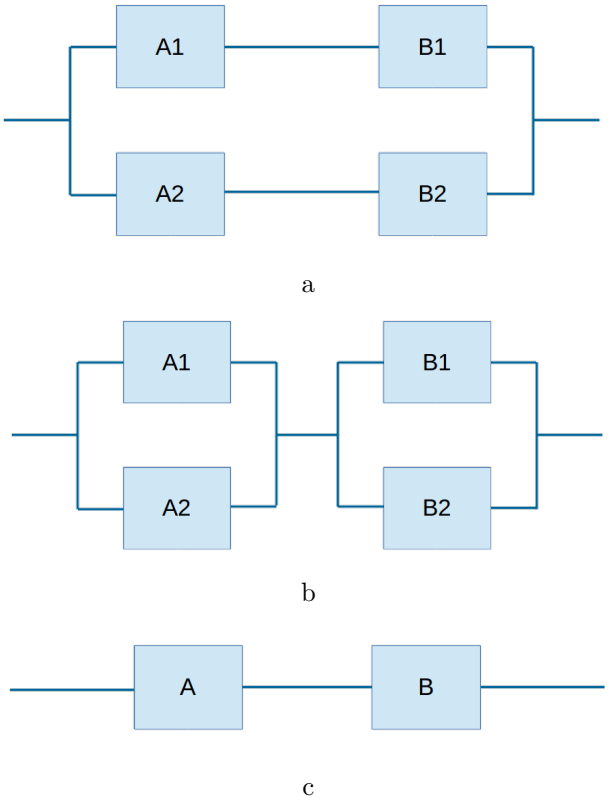

Figure 2.8: Schematic representations of the two components A and B arranged in architectures with varying levels of redundancy. a) Dual redundant power system. b) Fully redundant (cross-strapped) power system. c) Single string system

design consideration for satellites with high volume constraints such as CubeSats. Thus, such a design might be favoured in schedule-constrained projects with limited resources, e.g. educational nanosatellite projects. The failure probability of the fully-redundant (cross-strapped) system shown in Fig. 2.8b is given as the failure of both A components or both B components:

$$P_{F,b} = P(A_1 \cap A_2) \cup P(B_1 \cap B_2) = P_{A_1} P_{A_2} + P_{B_1} P_{B_2} - P_{B_1} P_{B_2} P_{A_1} P_{A_2} \quad (2.3)$$

The dual redundant power system shown in Fig. 2.8a offers a "middle ground" between the fully redundant and single-string systems. Its failure probability is

given as:

$$P_{F,a} = (P_{A_1} \cup P_{B_1}) \cap (P_{A_2} \cup P_{B_2}) \tag{2.4}$$

$$= P_{A_1}P_{A_2} + P_{A_1}P_{B_2} + P_{B_1}P_{A_2} + P_{B_1}P_{B_2} - P_{A_1}P_{A_2}P_{B2} + \tag{2.5}$$

$$- P_{B_1}P_{B_2}P_{A2} - P_{A_1}P_{A_2}P_{B_1} - P_{B_1}P_{B_2}P_{A_1} + P_{A_1}P_{A_2}P_{B_1}P_{B_2} \tag{2.6}$$

In order to compare the three systems, it is assumed that all the failure probability are equal:$P_{A_1} = P_{A_2} = P_{B_1} = P_{B_2} = P_A = P_B$. Then, by plotting the three equations for different failure rate, one can observe that $P_{F,b} < P_{F,a} < P_{F,c}$, i.e. that the fully cross-strapped system has the lowest failure probability of all three. However, this assumes that the connections between components A and B have the same failure probability as in the case of single-string system. This might not be the case if the connections are realised with harness, and are manufactured and tested by inexperienced students, for example [27]. Depending on the complexity of the circuits that components A and B require, the complexity of the complete A-B system in the fully cross-strapped configuration might reach a level where design flaws will be difficult to identify in a timely fashion, thus leading to an on-orbit failure or missing the launch window.

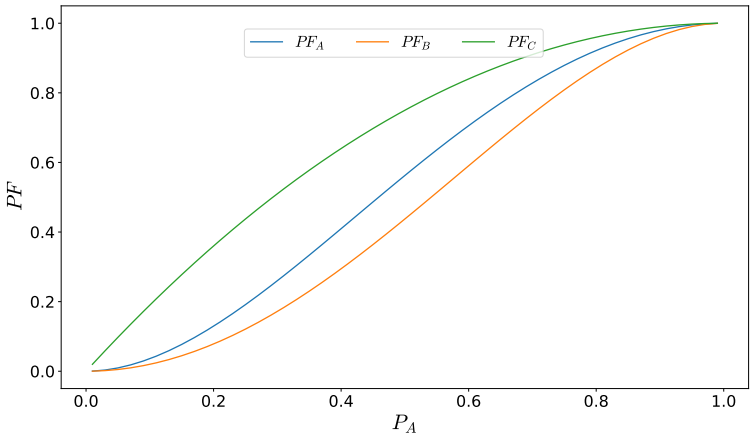

Figure 2.9: Failure probability comparison assuming all the components has the same value

Even though $P_{F,a}$ is theoretically higher than the failure probability of the fully

redundant system, $P_{F,b}$, the reduced system complexity might result in lower P_F in practice due to design errors and insufficient testing [27]. Still, $P_{F,a}$ of the dual bus system is less than the $P_{F,c}$ of the single string system. Moreover, if the secondary power system is scaled to only provide the power necessary to satisfy the primary mission objectives, as in the discussed case of the nanosatellite, the increase in reliability is associated with modest mass and size penalties, as opposed to implementing full redundancy. An extreme case of this design approach is Shinen-2 that, as shown in Fig. 2.6, consists of two single string systems, one of which is designed to operate a communications subsystem. This reduced the systems complexity to the minimum, while lowering the probability of failure of the telecommunications subsystem as a whole, i.e. failure of both communication lines.

2.5 Summary

The design and implementation of two electrical power systems were presented and illustrated using examples of a nanosatellite and a micro deep-space probe. Both systems had independent solar array inputs and independent battery arrays, thus the power conditioning unit was split in two separate units in both cases.

These two examples were cases of single-bus and dual-bus electrical power systems. On the one hand, for the case of the nanosatellite, the two PCMs were rated at different power output to a single-bus, making the secondary system a backup unit that enabled minimum functionality. On the other hand, the electrical power system of the micro deep-space probe was split in two almost identical units (EPS 1 and EPS 2). Each EPS had an independent power bus and, therefore, Shinen-2 operated using a dual-bus electrical power system that had two communication subsystems powered from different power buses.

Chapter 3

Modular approach for power generation in EPS[†]

Achievement of rapid development and low cost is necessary for the sustainability of small satellite programs. Using modular approach for the components of EPS allows the reduction in development time and cost. This chapter describes a module, called Solar Module Integrated Converter (SMIC), that integrates the solar cells and the power condition units. After the design and qualification of the SMIC, the required number of modules can be manufactured and integrated in the EPS. It is very difficult to have a unique design that can meet the requirement of all satellites, then, the guidelines for designing the modules have been proposed and described [9],

3.1 Introduction

In recent years, the number of developments and launches of small satellites has been increasing, attracting the attention of investors seeking new businesses and of universities wanting to use them for research and educational purposes [4, 28, 29].

[†]This chapter is based on the second publication of this thesis: 'Solar Module Integrated Converters as Power Generator in Small Spacecrafts: Design and Verification Approach.' by **Gonzalez-Llorente, J.**; Lidtke, A.A.; Hatanaka, K.; Kawauchi, R.; & Okuyama, K. *Aerospace* 2019, 6(5), 61., available at https://doi.org/10.3390/aerospace6050061 under a Creative Commons Attribution license CC BY 4.0

In all cases, rapid development and low cost are required by stakeholders to support a satellite mission. In addition, a failure rate reduction has become crucial to the sustainability of the space programs [30, 31].

One way to achieve both rapid development timelines and high reliability is by using a modular approach [23, 32]. The Electrical Power System (EPS), responsible for power generation, storage and regulation, is particularly suitable for modular implementation [33]. EPS is usually composed of solar array, battery, power control and regulation, and distribution and protection components [18]. Each of these components can be modularized so that the design and development of the EPS become fast and reliable.

Due to the cost of solar cells and its importance, one of the most crucial steps in the design of the EPS is the design of the solar array. For this, the number of solar cells and their arrangement, in series or parallel connections, must be determined to satisfy the power requirements [34]. Usually, various solar arrays of different sizes and arrangements are used in a single satellite [16, 35, 36]. Another design approach is using one large solar array providing most of the power [37]. These approaches have several disadvantages. Firstly, the design of the solar array becomes more complex, as the number of possible sizes and arrangements is high and each one needs a specific design. At the end, this increases the possibility of errors introduced at design time. Secondly, the EPS becomes less reliable; if one of the largest solar arrays fails, the satellite power is compromised. Thirdly, the efficiency of large solar arrays is not optimal because each cell is exposed to different radiation and temperature, but their set point is the same [34]. Lastly, when different designs are used, additional time is required for qualification and testing.

In contrast, using solar array modules of the same, modest size and identical arrangement can increase the performance and reliability of the EPS, while reducing the development time. The performance is increased because the peak power of each solar array can be extracted by its own power regulator that implements maximum power point tracker; conversely, one power regulator for a solar array with

different temperature and characteristics will extract less power [34]. Reliability is also increased by connecting two or more components in parallel [18]. Thus, EPS reliability is increased using solar array modules; if one solar array module fails, there are still other modules working as power source. Considering that identical modules will be used, the development time is reduced because the qualification process is done only one time. There is no need to qualify several designs. Then, the required number of identical modules will be manufactured and only the acceptance test is necessary, not the qualification test.

If a modular solar array is used, the design of the other components of the EPS can be realized independently, only including the number of required modules based on power requirements. Moreover, using the modular approach, power generation is decoupled from the rest of the EPS design [38]. However, designing a solar array module is not a trivial task. Ideally, the module must be scalable and easy to integrate; it must have a low cost, high efficiency and high reliability. However, these ideal features are usually in conflict, thus it is common to perform a trade-off.

Solar modules have been previously proposed in literature [33, 37, 39, 40]. The proposed designs for the power generation module vary in complexity. The modules proposed in [39, 40] only integrate the solar array while power regulation and housekeeping measurements are proposed as a different module. Integrating these three functions (solar array, power regulation and housekeeping measurements) in a single module increases the level of abstraction of the module, making the EPS design easier. One such module is proposed in [33]. However, their power regulation does not manipulate the solar array operating point to achieve maximum power. The design in [37] integrates the solar array and housekeeping but no power regulation, however, this design includes a magnetic actuator for attitude control.

The design of a modular solar power generation component including solar array, power regulation and measurements, depends on the satellite size and its voltage and current requirements. Therefore, a single module design will hardly fit a different satellite than that for which it was designed, and new missions need to design

their own modules. As previously mentioned, this is not an easy task as it involves a large combination space and many relationships among the different decisions to be made. For this reason, the objective of this study was to provide design considerations and a verification process for electric power system modules by integrating the solar cells, the power regulator and telemetry acquisition units to reduce the development time of small spacecraft while adding redundancy in the power source. The novelty and significance of this study is the proposal of a design and qualification approach for Solar Module Integrated Converters (SMICs), which can be used as a guide for new missions to design and evaluate a solar module for power generation easily.

The contributions of this chapter are as follows:

- We propose a Solar Module Integrated Converter to integrate the solar array, the solar array regulator with peak power tracker and the measurement circuit in a single module (Section 3.2.1).
- Since we understand that a single design is hard to realize, we propose a design and qualification method for SMIC that can be used to adapt the sizing of each module to a particular mission (Sections 3.2.2 and 3.2.3).
- We applied the proposed method to the design and qualification of the SMIC for Ten-Koh satellite, showing how the proposed SMIC and methods were used in specific mission design (Section 3.3).
- We present results of Ten-Koh Solar power generation flight data recorded during operation in-orbit, which verifies and validates the proposed SMIC and design approach (Section 3.4).

The SMIC module for Ten-Koh satellite integrates power generation with triple junction solar cells, solar array regulation based on peak power tracking, and measurements for housekeeping data collection that include current, voltage and photo-diode for sun incidence angle estimation. The designed module was qualified

for space use following the proposed verification method and integrated into the quasi-spherical satellite Ten-Koh launched on 29 October 2018. The satellite and its SMIC are shown in Figure 3.1. Twelve identical modules were integrated to Ten-Koh satellite, which has been operating continuously for five months.

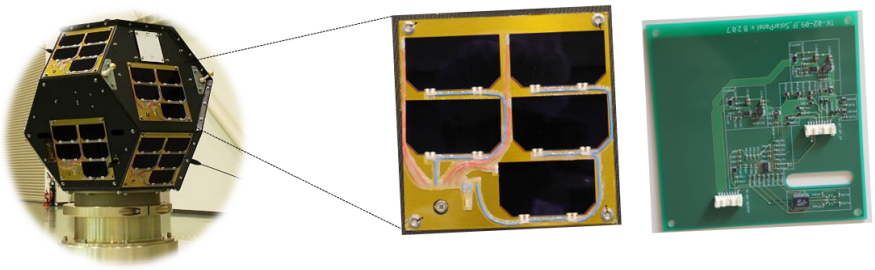

Figure 3.1: Solar Module Integrated Converter applied to Ten-Koh satellite: external view with solar cells and internal view where PCB with solar array regulator is shown.

3.2 A Modular Design Approach for Solar Array

In this section, we describe the proposed architecture for a solar power generation module (Section 3.2.1), named Solar Module Integrated Converter (SMIC). As stated in Section 3.1, a " silver bullet" module design that fits satellites with different sizes, shapes and power requirements does not exist. Therefore, we detail some design considerations to guide the design of SMIC for specific mission requirements. Finally, we delineate a validation and verification plan for such SMIC.

3.2.1 SMIC Architecture

The EPS of a satellite is responsible for generation, storage and distribution of power. In this chapter, a modular architecture and design approach for the power generation function is proposed. The proposed SMIC defines a core array that can be used to create a multi-array of solar cells (Figure 3.2). Each module also contains the solar array regulator (SAR), thus it becomes a plug-and-play energy source ready to be integrated with the rest of the EPS. We also propose to include

the sensors and interfaces for housekeeping data generation and communication into the SMIC (Figure 3.3). This makes the entire power generation part of the EPS arbitrarily scalable while minimizing the impact on the rest of the satellite system.

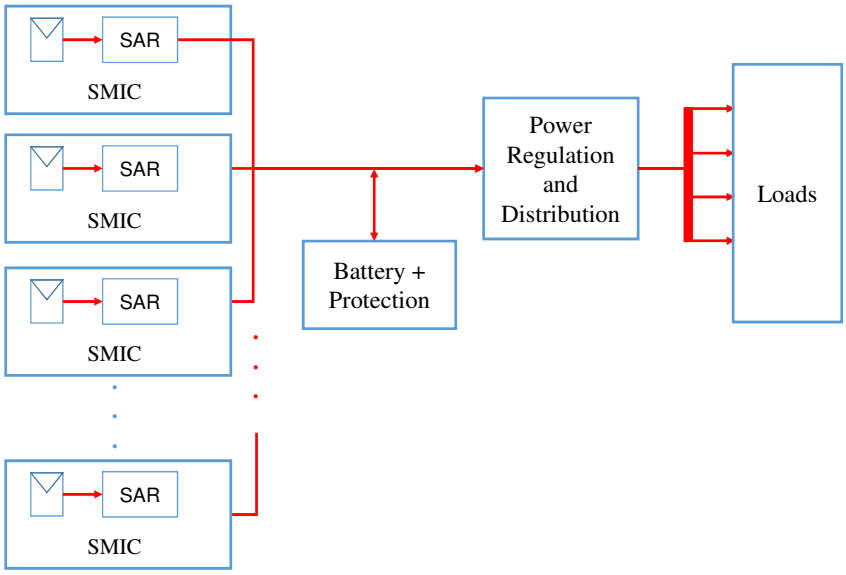

Figure 3.2: Architecture of EPS with multi-array of solar cells using Solar Module Integrated Converter (SMIC).

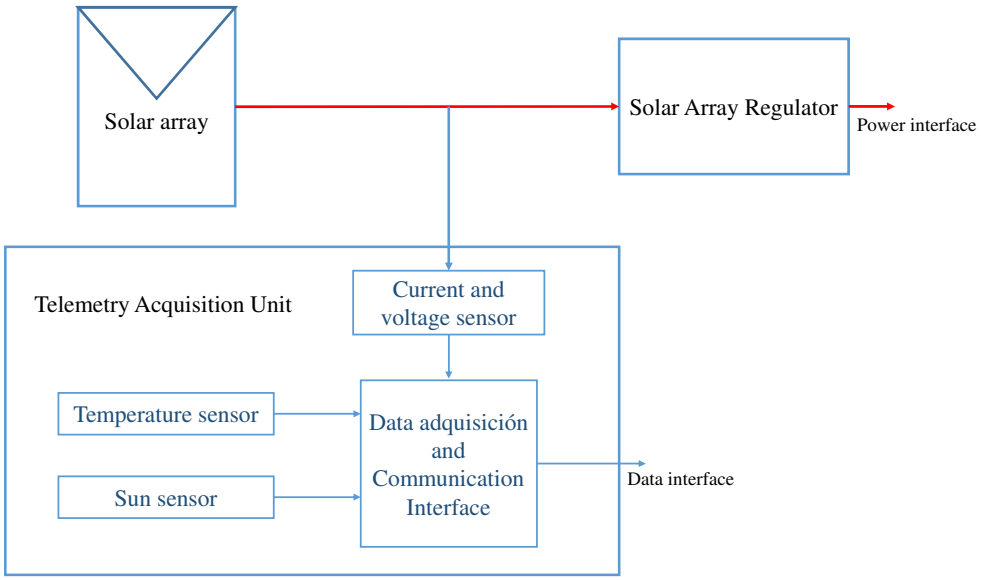

Figure 3.3: Architecture of Solar Module Integrated Converter (SMIC).

Thanks to using a modular approach, the development time is reduced and power

generation efficiency can be increased as compared to a typical configuration where multiple solar array designs are used. In summary, the advantages of the modular approach are the following:

- By designing a module, the design and implementation become easier and the designed solar array can be reused in each face of the satellite.
- All verification and validation tests can be done on a single module instead of all installed modules.
- The power output of each solar array will be optimized even if they have different radiation and temperature conditions.

The following subsections describe each component of the SMIC.

3.2.1.1 Solar Power Generation Unit

This component is the energy source of the spacecraft, which for small satellites tends to be derived from solar arrays. A solar array is formed by connecting several solar cells in series, parallel or series-parallel. Series connection is used to increase the voltage of the SMIC. Parallel connection is used to increase current and avoid losing the string when one solar cell of the array is damaged [41]. A series-parallel connection combines both objectives.

As shown in Figure 3.2, two or more SMICs can be connected together to meet the total power requirements of the satellite mission. As in the case of solar cells, SMICs are connected in series, parallel or series-parallel following the same logic. In the design approach section (Section 3.2.2), we describe how to make the decisions of the number of cells and type of connection to use.

3.2.1.2 Solar Array Regulator

The Solar Array Regulator (SAR) has two main functions. The first one is to match the solar array and the load to obtain the maximum power available from the array. Even when the solar cells receive the maximum irradiance, the power generated from them can be minimum if there is a load mismatch. The second function of the SAR is to prevent the batteries from overcharging by controlling the power generated by the solar array according to their charge state.

There are mainly two approaches for solar array regulators to obtain the maximum power given a condition of temperature and sun incidence angle: Direct Energy Transfer and Maximum Power Point Tracker (MPPT) [18, 42]. Both can achieve a load matching to obtain maximum power from the solar array. However, DET can obtain the maximum power just for one specific condition while MPPT can continuously track the maximum power point.

Both techniques of solar regulators can be used in a modular approach [33]. In the proposed SMIC architecture, we chose to implement MPPT because it offers several advantages compared to DET. Firstly, MPPT allows the use of solar arrays with different voltage levels, thus it can be used in different EPS. Secondly, the power output of each solar array will be optimized even for different radiation and temperature [43]. Thus, MPPT is optimal when installed in satellites using body mounted solar cells, in which each side experiences different conditions. This is equivalent to having a distributed photovoltaic system [44, 45].

3.2.1.3 Telemetry Acquisition Unit

This component is responsible for measuring the operating conditions of the whole SMIC. These measurements must be provided to the satellite data handling subsystem through a data interface such as I2C, SPI, etc. [46]. The most important measurements to monitor the health condition of the solar panels are their currents,

voltages and temperatures. Sensors for measuring these variables must be installed in the SMIC.

Besides measuring the health of the energy source and the satellite itself, other sensors can also be installed in the SMIC to obtain additional data about the operating conditions. For example, the sun incidence angle on each solar panel can be measured by installing sun sensors in the SMIC. The measurements provided by this component can be used for other purposes in the satellite mission, e.g., including satellite attitude estimation [47].

3.2.2 SMIC Design

We now move on to the design approach for the SMIC. During the SMIC design, decisions about which exact solar cells will be used, the number of solar cells in each array, how the cells are connected, the topology of the MPPT and which sensors will be installed must be made. These decisions are tightly coupled, thus changing one variable will affect the decision for all others. Moreover, the number of possible values for every decision can be high. Thus, designing the SMIC can become a difficult task. The purpose of this section is to provide a guideline for designers to facilitate the process, focusing on the design of the solar array regulator and the power generation component. Selection of telemetry sensors should be done according to the desired measurements.

3.2.2.1 Design of Solar Array Regulator

We propose to begin the design by defining the Solar Array Regulator (SAR). The SAR choice will restrict the maximum voltage that can be provided by the Power Generation Component [34]. This restriction is mainly given by the choice of the topology of the MPPT. Thus, selecting one topology with high efficiency is a key element in the design process [48]. The main topologies are buck converter, boost converter or buck-boost converter. Other topologies such as SEPIC or Cuck

are popular for implementing MPPT in direct current power systems, but we only discuss the implications in the design of the main topologies.

When choosing the buck-converter topology, the voltage must be higher than that of the batteries. When choosing the boost converter, the voltage must be lower than that of the batteries. We assume the battery has been selected previously, thus this voltage is known and considered a constraint for the design.

When choosing the buck-boost converter, there is no restriction in terms of voltage related to the battery. However, it still has the restriction of the maximum rating, meaning the maximum operating voltage and current. This restriction also applies to the buck converter and to the boost converter.

3.2.2.2 Design of Solar Power Generation Unit

The next step in the design process of the SMIC is designing the solar array. This is the most important step because it determines the power available from the module. There are three decisions to be made: (1) the solar cells to be used; (2) the number of cells in each module; and (3) connection between the cells. This is an iterative process as one decision can be updated based on the results of later decisions.

The type of solar cells is decided based on mission constraints, most notably the budget and availability of the cells on the market. Nowadays, commercially-available triple-junction solar cells can achieve efficiency of up to 30 % and they are commonly manufactured in sizes around 30 cm^2 and 26 cm^2 [49–51]. An initial type of solar cells can be chosen to continue with the design. It can be updated later if the power balance is not met with the chosen cells, or if lower-cost cells can provide sufficient power.

After choosing the type of solar cells, the number of solar cells to be installed must be decided. To choose the number of cells in each module, we must first know the total number of cells that will be installed in the satellite. The typical approach

for CubeSats and small satellites without deployable solar arrays is to cover the maximum area of external surface with solar cells. However, this approach can be costly and lead to an over-sized array. Conversely, if the number of installed solar cells is not enough to operate the satellite, the mission is not feasible. To avoid a high cost, the number of cells on each side can be determined by doing an energy balance.

The energy balance is obtained by matching the satellite power requirements with the power generation. Power requirements of the mission determine the total number of solar cells mounted on the satellite because the amount of power generated is directly related to the number of solar cells. The total solar power generated is approximately the sum of the power generated by each module

$$P_{solar} = \sum_{j=1}^{m} P_{module_j}(A_{SMIC}, \gamma_j) \tag{3.1}$$

where m is the number of SMICs and $P_{module_j}(A_{SMIC}, \gamma_j)$ is the power generated by the module number j, which is a function of the area covered by the cells in the SMIC (A_{SMIC}) and the incidence angle of the sun with the module (γ_j).

Specifically, assuming that the maximum power can be obtained, the power generation of a solar module, P_{module}, depends on the illuminated area of the module, $A_{SMIC} \cdot \cos(\gamma_j)$, and is given by

$$P_{module} = S_0 \cdot \epsilon_{cell} \cdot A_{SMIC} \cdot \cos(\gamma) \tag{3.2}$$

where S_0 is the solar constant given by the orbit, ϵ_{cell} is the efficiency of the solar cells [52]. Considering the illuminated area is a function of the incidence angle, the power generated by each module can be different, especially in satellites with body mounted solar cells [53]. In this case, sides with different solar incidence angle will generate different power.

An initial number of cells in each SMIC can be determined by the available area to install each module. In the case of body mounted solar cells, as is the case for most small satellites, this area is given by the satellite structure. This area is divided by

the solar cell area to determine the number of cells to be considered. After this, the generated power is calculated and the number of cells can be adjusted accordingly. If the power generated is too high, the number of cells in each module, or the number of modules, can be reduced. If the power generated is too low, then the type of solar cells should be changed for one with more efficiency.

Since the incidence angle depends on time, the generated power used for evaluating the design can be obtained based on the average power by simulation. Another approach to calculate the generated power can consider only the scenario of minimum power generation when the illuminated area is minimum; this case is simpler and more conservative. The generated power is used for adjusting the number of cells based on energy balance.

Once the number of solar cells is defined, the electric configuration of the solar array is determined by the input requirements of the solar array regulators. In this way, the maximum voltage or maximum current of the SAR are respected to ensure its safe operation. The voltage range of the SAR determines the number of cells that can be connected in series. This can be set as an initial constraint. The array is completed by connecting the cells in parallel without exceeding the current rate of the SAR.

3.2.3 SMIC Verification Approach

The goal of the verification process is to confirm that the SMIC is able to withstand the vibration and shock experienced during launch, and the thermal cycling expected in orbit. This is to say that the mechanical and thermal-vacuum conditions should not affect the functions of the SMIC, or reduce its performance. As presented in Section 3.2.1, the SMIC can be split into three functional units:

1. Solar array;

2. SAR; and

3. Telemetry Acquisition (TMA) unit.

The solar array is likely orders of magnitude more expensive than SAR and TMA units due to the high cost of space-grade solar cells relative to Commercial of-the-shelf (COTS) integrated circuits, which form the backbone of the SAR and TMA units. It is, therefore, desirable to reduce the number of Qualification Models (QMs) of the solar array units and to reduce the amount of testing that they are subjected to, in order to reduce the overall project cost. However, the qualification process should be as complete, and representative of the launch and flight conditions as possible to ensure that the flight SMIC will correctly function in orbit.

One way to address this reliability–cost–risk trade-off is to use the Proto-Flight Model (PFM) approach in the qualification of the SMICs. However, if this approach is followed, eventual design flaws cannot be rectified without re-working all PFMs close to the launch date, which will have a cost and schedule impact on the project. In the case of piggyback satellites, it could even mean missing the launch opportunity altogether. To mitigate the risk of missing the launch, the qualification approach depicted in Figure 3.4 is proposed for SMICs.

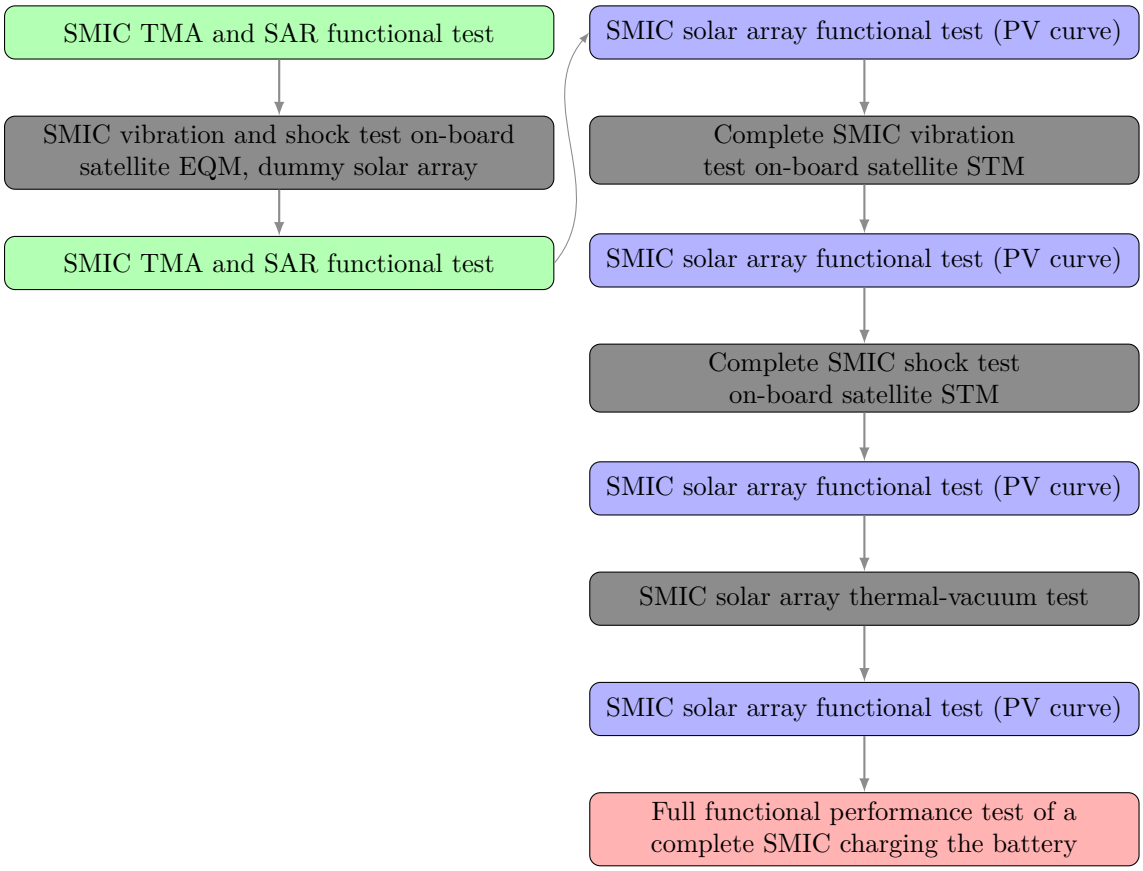

Figure 3.4: The sequence of qualification tests proposed to the SMIC. In the sequence of the tests on the left, solar arrays are not included in the tests to reduce the risk of damaging the expensive solar cells. Only the TMA and SAR units of the SMIC are tested there, shown in green. Solar arrays are tested in the sequence on the right, with PV curves obtained at the purple steps in the process. The complete SMIC was functionally tested with the battery at the end of the qualification process, shown in red.

First, the qualification models of the SMIC TMA and SAR units need to be tested with the rest of the satellite during the system-level qualification campaign. Functionality of the units should be verified before and after mechanical testing (green blocks in Figure 3.4) to ensure that they can survive the launch without loss of performance. At this stage, dummy masses of the solar arrays can be used and the vibration spectra on them should be measured.

The measured vibration spectra must then be compared to the solar array natural frequency (ω_N) computed using a finite element model (FEM), in order to

assess whether ω_N of the solar array is above the peak of the vibration spectra, i.e., whether the solar array is likely to withstand the vibration environment. Once this is confirmed, one qualification model of the solar array can be manufactured, and a complete SMIC will be subjected to qualification mechanical and thermal vacuum testing (right-hand side of Figure 3.4). To confirm no damage has been sustained by the solar array throughout the qualification testing, current–voltage curves of the solar cells should be measured before and after each test (blue blocks in Figure 3.4). The curves can be obtained by measuring the current and voltage while the load is changed when the solar array is illuminated at constant irradiance [54]. At the end, the SMIC should be functionally tested in an integrated subsystem test to ensure that it correctly interfaces with other components of the EPS.

3.3 Applying Solar Module Design to Ten-Koh Satellite

In this section, we use Ten-Koh satellite as a case study to apply the proposed guidelines to the design of the SMIC.

3.3.1 Power Needs and Constraints for Case Study: Ten-Koh Satellite

The main function of the solar array is to provide the power required by satellite bus and payloads to achieve the satellite mission. The solar array is designed under two constraints: (1) the orbit that determines the amount of solar irradiance and the time of sunlight and eclipse; and (2) the geometry of the satellite that determines the operating conditions of the solar array, for example, its incidence angle.

3.3.1.1 Satellite Orbit

As mentioned above, the orbit determines the sun intensity or solar irradiance received by the satellite. Ten-Koh satellite was launched as a piggyback payload of GOSAT-2 into a sun-synchronous, sub-recurrent orbit. The initial orbit altitude, h, was 613 km and the orbit period, τ, was 5817 s (about 1.6 h). This can be calculated as

$$\tau = 2\pi\sqrt{\frac{(h+r_e)^3}{\mu}}, \tag{3.3}$$

where μ is the Earth gravity parameter (398,600.44 $\text{km}^3 s^{-2}$) and r_E is the mean Earth radius (6378.14 km).

This orbit determines that the average irradiance received by Ten-Koh is 1367 W/m^2, the solar constant, S_0. This is the solar energy potential that reaches each SMIC on the spacecraft. However, the generated power per SMIC (P_{module}) is determined by its angle in the spacecraft (that defines the incidence angle, γ) and the number of solar cells (that defines the area covered by the cells, A_{SMIC}) as given by Equation (3.2). Then, the total energy produced during each orbit period is calculated using the total solar power generated (P_{solar}, from Equation (3.1)) and the sunlight time. From the satellite orbit, the sunlight time and eclipse time are 3715 sand 2092 s, respectively. Thus, the satellite is receiving sunlight during 63 % of the orbit. Section 3.3.3 shows the calculation for the spacecraft orientation with the worst condition to determine the number of solar cells in the SMIC considering the minimum energy generation.

3.3.1.2 Power Requirements

The power required by satellite subsystems to operate must be provided by the solar array. Ten-Koh platform has the following subsystems: on-board computer (OBC), two redundant communications subsystems (COM-1 and COM-2), Attitude Determination Subsystem (ADS), and Electrical Power Subsystem (EPS). Secondary Payloads (PL-2) and Primary Payload Components are: Experiment

Control Unit (ECU), Double Langmuir Probe (DLP) and Charge Particle Detector (CPD). Table 3.1 shows the power required by each subsystem during operation.

Table 3.1: Power consumption of Ten-Koh subsystems.

Subsystem	**Nominal Power (W)**	**Peak Power (W)**
OBC	0.50	0.70
COM-1	0.50	3.20
COM-2	0.50	3.20
ADS	1.00	2.00
EPS	0.60	1.00
ECU	1.20	1.70
DLP	1.40	2.05
CPD	5.00	5.30
PL-2	1.50	2.50

As many satellites, Ten-Koh has different modes of operation. Each mode determines which subsystems are powered on, while the others remain turned off. Therefore, energy balance for different operating modes can be analyzed by combining the power and the duration of the corresponding operating mode.

In Table 3.1, the CPD mission is the subsystem with the highest power consumption. This mission is operated for at most 32 min in one day. We used a scenario of one-day operation with CPD mission to design the Ten-Koh SMIC. The total power required to power the spacecraft during nominal mode is 3.3 W and 9.5 W during CPD mission. Then, the minimum energy required to execute the mission is 9.5 Wh.

3.3.2 Solar Array Regulator

The solar array regulator (SAR) used in the module is based on Maximum Power Point Tracking (MPPT) to optimize the power generation of the solar cells. Table 3.2 shows the requirements for normal operation of the selected MPPT (SPV1040).

Table 3.2: Maximum electrical ratings of the selected MPPT.

Parameter	**Value**	**unit**
Maximum input voltage	5.5	V
Maximum output voltage	5.2	V
Maximum input power	3.3	W
Maximum output power	3.0	W
Maximum input current	1.8	A

As mentioned in the design approach, the topology of the dc-dc converter is a constraint for design the solar and battery arrays. In Ten-Koh, the MPPT selected is based on boost converter, thus the voltage of the solar array must be lower than the battery array. Ten-Koh battery array voltage can vary between 3.1 V and 4.1 W.

3.3.3 Solar Array Configuration

We designed the Ten-Koh SMIC as a module for a solar array that can be installed on both hexagonal and square faces of the satellite. Therefore, the maximum number of solar cells in each SMIC is determined by the smallest side of Ten-Koh. This is the square face with length of 15.2 cm, which has an area of 231 cm^2.

With this area in mind, we selected the solar cells to be installed. The electric characteristics of commercial solar cells are listed in Table 3.3. The cells with 26.5 cm^2 were selected to cover more area in the module and have more power generation.

Table 3.3: Parameters of triple junction cells for cells of 26.5 cm^2 and 30.15 cm^2 for standard conditions (1367 W/m^2, 28 °C).

Parameter	**26.5 cm^2**	**30.15 cm^2**
Short circuit current, I_{sc}, (mA)	473	538
Open circuit voltage, V_{oc}, (mV)	2.60	2.61
Current at maximum power, I_{mp}, (mA)	455	517
Voltage at maximum power, V_{mp}, (mV)	2.32	2.33
Maximum length (mm)	69.1	80.15
maximum width (mm)	39.7	40.15

By simple area analysis, we can install up to eight cells in each module. However, considering the space of the terminals of the solar cells, and the space for temperature and sun sensors, we could only install six cells in the module. If solar cells of 30.15 cm^2 were selected, then three solar cells could be installed in the module.

Using the worst case scenario, we considered a case when solar radiation is perpendicular to the top side of Ten-Koh, which has no SMIC installed (Figure 3.5). This is the same case as when solar radiation is perpendicular to Ten-Koh launcher adapter ring. In this scenario, only six modules receive solar irradiance at an angle of 70 degrees for the hexagonal and 55 degrees for the square faces. This analysis gave us a total power of 13.18 W and, considering the sunlit time of the orbit, the minimum energy generation of 13.5 Wh. This exceeded the needs of Ten-Koh (9.5 Wh). Therefore, we decided to use only five cells, which still satisfied the energy balance. In the worst case, the generated power with five cells per module was 10.98 W. Thus, the minimum energy generation is 11.30 Wh, which was enough to meet Ten-Koh energy requirement.

Table 3.4 shows the comparison of the number of cells for the three cases previously described. Using the modular and power balance design approach, we reduced costs and development time in Ten-Koh.

Table 3.4: Comparison of the number of cells for three design approaches: maximum area approach vs. modular approach with area analysis and power balance.

Approach	**Amount of Cells in Hex. Side**	**Amount of Cells in Square Side**	**Total**
Maximum area covered of cells	12	5	102
Modular approach with area analysis	6	6	72
Modular approach with power balance	5	5	60

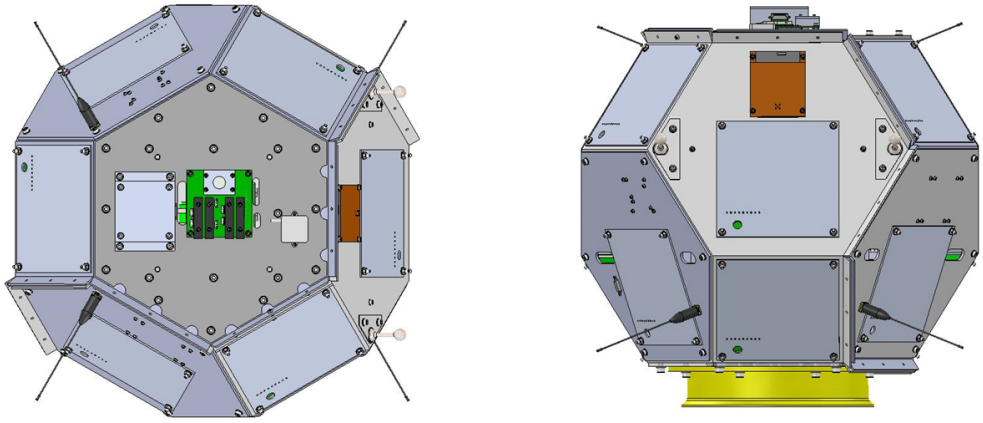

Figure 3.5: Two orientation scenarios of Ten-Koh satellite: (**Left**) worst-case scenario for power generation because the least area is exposed to solar radiation; and (**Right**) best case for power generation. The launcher adapter ring is shown in yellow.

Once the number of cells was decided, it was necessary to define the electrical configuration of the array. Because the maximum voltage of SAR is 3.7 V, no series connection can be made, as two serial cells would give a maximum voltage of 4.6 V, which is higher than the battery voltage (4.2 V). This resulted in a parallel connection of all cells.

Although all five cells could be connected in a parallel configuration, no commercially available solar array regulator could handle the total power of five cells (see Table 3.2). For this reason, we connected two arrays in each SMIC: one array of two cells in parallel and the other with three cells in parallel. In these two sub-arrays, the solar cells are connected in parallel by using near-ideal diodes (LTC4412) to

prevent a single cell with a short-circuit from disabling an entire array. The only difference between both arrays is the provided current.

3.3.4 Solar Module Measurements

As for measurements, we decided to include voltage, current, temperature and sun incidence angle. One temperature sensor and one four-quadrant photodiode were installed on the external side of the SMIC. The internal side included two current sensors and one voltage sensor for power monitoring. All sensors provided analogue outputs.

A high speed, low power analog to digital converter (ADC) was used for data acquisition of the measurements of the solar module (AD7927). The converter includes one serial interface (SPI) to transmit the conversion results of the eight analog inputs to a microcontroller.

As explained above, there are two sub-arrays in every module, one with two cells and the other with three cells. The output current of every array is measured by using a shunt resistor with a current-sense amplifier. Only the voltage of the array with three cells is measured to have more channels available for attitude determination sensors and without increasing the required number of ADCs.

A two-terminal linear temperature transducer (AD590) that does not require cold junction compensation or special signal conditioning circuit was used to measure the external temperature of the solar panel. A current-to-voltage conversion resistor was used to couple the output to the input of the ADC.

A COTS quadrant Si PIN photodiode (S4349) was mounted on every solar module. The photodiode was aligned with the plane of the solar module; in this way, its output is related to the incidence angle of the solar irradiance. The four outputs are converted to voltage and connected to the ADC.

3.4 Experimental Results of SMIC

The SMIC developed for the Ten-Koh satellite was qualified for space use according to the scheme put forward in Section 3.2.3. The present section summarizes the results of mechanical and thermal vacuum qualification testing, as well as the related functional testing.

3.4.1 Mechanical Qualification

During the Ten-Koh system qualification campaign, the satellite engineering qualification model (EQM), which included dummy masses of the solar panels and EQMs of the remainder of the SMICs, was tested mechanically following the flow given in Figure 3.6 and according to the test conditions specified in Table 3.5. Qualification levels were used in this testing in accordance with the JAXA standards, meaning that the loads that were applied on the satellite EQM were more severe than during the launch. Note that modal surveys between consecutive tests were omitted from Figure 3.6 for brevity. These surveys (0.5 Grms random vibration tests) were used to assess whether the EQM had been damaged and whether to continue the testing. The functionality of the EQM SMICs, excluding the solar arrays, was verified before and after the system EQM tests to ensure that they can survive the launch environment. No mechanical testing was conducted on any part of the SMICs on their own to reduce the time required for the overall Ten-Koh test campaign.

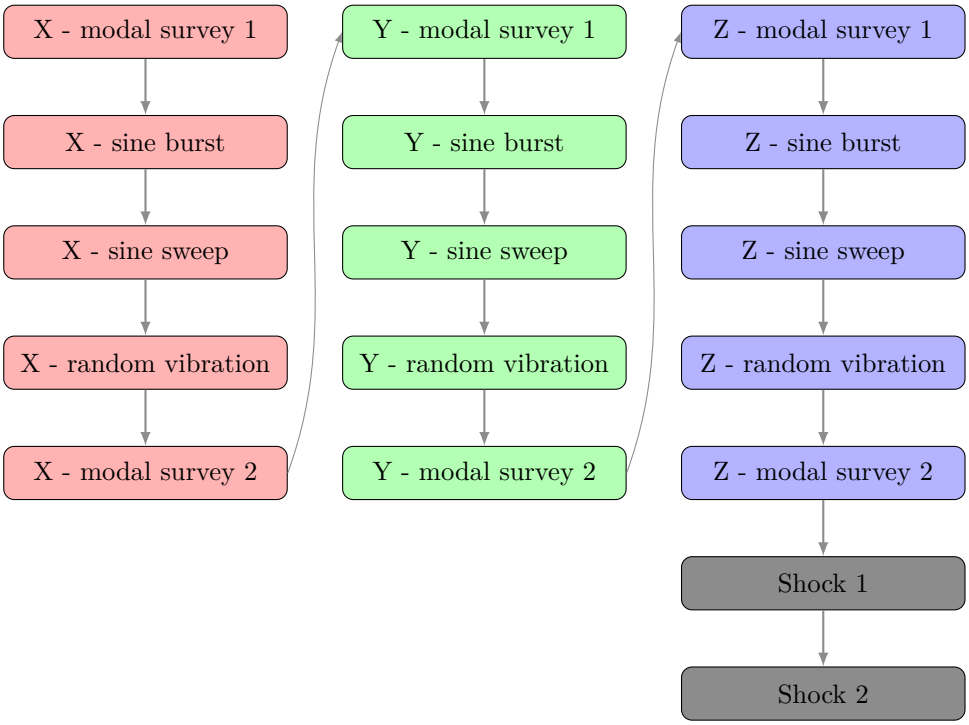

Figure 3.6: The sequence of mechanical tests conducted on the qualification model of the solar panel. The same sequence also applies to the satellite EQM test, but modal survey was carried out after each test during the satellite system-level tests.

Table 3.5: Mechanical qualification test conditions used to test the SMIC. X refers to the satellite longitudinal (aligned with the launch vehicle acceleration) axis, while Y and Z axes complete the orthogonal triad.

Test	**Condition**	**Value**
Shock (all axes)	SRS 100 to 2600 Hz SRS 2600 to 5000 Hz No. shocks	+6 dB/octave 2000 G 2
Sine burst (all axes)	Frequency Acceleration No. tests	20 Hz 7.5 G 1
Sine sweep (S/C X-axis)	Frequency Acceleration Sweep rate	5 to 100 Hz 3.13 G 2 octave/min
Sine sweep (S/C Y and Z-axes)	Frequency Acceleration Sweep rate	5 to 100 Hz 2.5 G 2 octave/min
Random vibration (all axes)	PSD 20 to 200 Hz PSD 200 to 2000 Hz Duration RMS acceleration	+3 dB/octave 0.064 G^2/Hz 120 seconds 11 Grms

After the satellite EQM tests, the vibration environment on each face of the satellite was analyzed and the 2-norm of the power spectral density (PSD) was computed for each face as per Equation (3.4):

$$|PSD| = \sqrt{PSD_X^2 + PSD_Y^2 + PSD_Z^2}. \tag{3.4}$$

In Equation (3.4), X, Y and Z represent the orthogonal axes of the SMIC reference frame, along which the acceleration was measured during the satellite EQM tests. The most severe, from the point of view of the solar array, face was chosen by finding the face with the largest $|PSD|$ at the natural frequency of the solar array (FEM result, 315 Hz). This PSD, together with the natural frequency of the solar array part of the SMIC is shown in Figure 3.7.

The structural-thermal model (STM) of Ten-Koh was then assembled and fitted with 11 dummy masses of the SMICs, and one qualification model (QM) of the

complete SMIC (including the solar array) located on the face with the most severe vibration environment. This setup is shown in Figure 3.8. This was done to reduce the number of solar panel QMs (reduce the cost) but to ensure that the complete SMIC will be qualified to the highest expected levels (high reliability). The SMIC was tested while mounted on the satellite to ensure that correct vibration and shock environments were applied to it, which would be difficult to achieve otherwise given the non-orthogonal orientation of the satellite faces with respect to the satellite axes.

The sequence in Figure 3.6 was then repeated by applying the qualification test conditions in Table 3.5 to the satellite STM. However, this time only the modal surveys indicated in Figure 3.6 were performed to reduce the testing time. At that point, the STM had already been qualified and it was expected to withstand the mechanical tests. The functionality of the SMIC, this time including the solar array, was verified before and after the vibration and shock tests, which is described in Section 3.4.3. During these two series of tests, all parts of the SMIC were subjected to the complete mechanical testing specified in Table 3.5.

Overall, the difference in cost of the two SMIC sub-assemblies, the solar array and the SAR+TMA unit, was leveraged to achieve full qualification while minimizing the number of solar cells used in the process. Notwithstanding the use of dummy solar panels in certain steps, the entire SMIC was subjected to mechanical qualification testing. Note that the mechanical test facilities were used for longer than they would have been if PFM approach had been followed. This was because such facilities were readily available at Kyutech and their use did not considerably affect the project budget relative to procurement of solar cells. For other projects, the rental costs of test facilities might make the PFM approach more viable from the budget point of view.

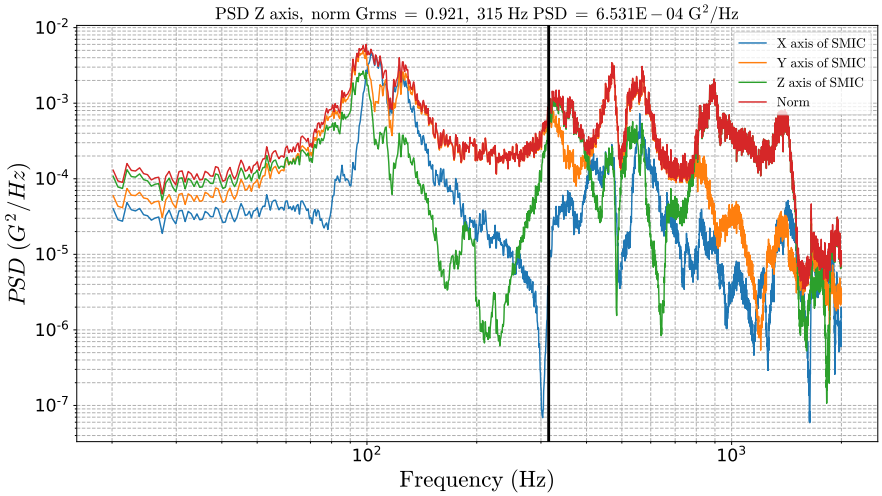

Figure 3.7: Power spectral density applied to the SMIC. Showing the natural frequency of the solar array derived using finite-element modelling (315 Hz) with a black line. $|PSD|$ shown in red, PSDs measured along individual SMIC axes in other colors.

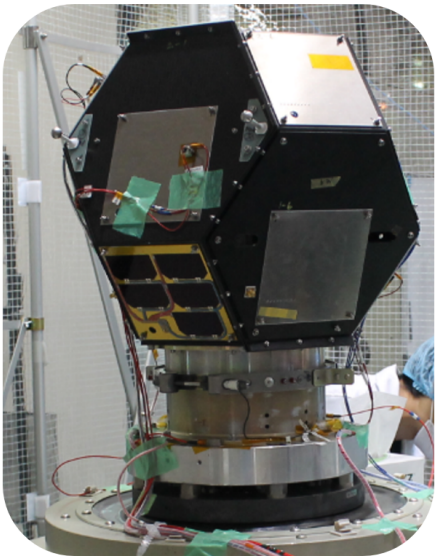

Figure 3.8: SMIC setup in Ten-Koh STM during vibration.

3.4.2 Thermal Vacuum Qualification

The Thermal vacuum (TVAC) qualification was defined as minimum of three cycles of hot (45 °C) and cold (−30 °C) temperatures at a pressure lower than 1.3×10^{-3} Pa. Dwell of at least one hour was required when the target temperature

became steady. The heating and cooling rate was controlled to prevent a thermal shock, keeping a rate around 3 °C/min.

Figure 3.9 shows the setup of the SMIC in the vacuum chamber and the heater that was powered by a controlled power supply from a computer with LabVIEW program. The computer also registered the measurements of temperature and pressure. Figure 3.10 shows the history of the temperature and pressure measured during the thermal vacuum for 3.5 cycles. The first cooling from room temperature is not shown for brevity. After the third cycle, the chamber was returned to normal pressure and to room temperature after a brief heating to avoid condensation after the opening of the chamber door.

The duration of hot and cold dwells varied because the satellite battery was being tested in the same chamber at the same time and it required a longer time to reach the dwell temperature. However, the duration was always longer than the minimum required duration (one hour). Dwell durations are summarized in Table 3.6.

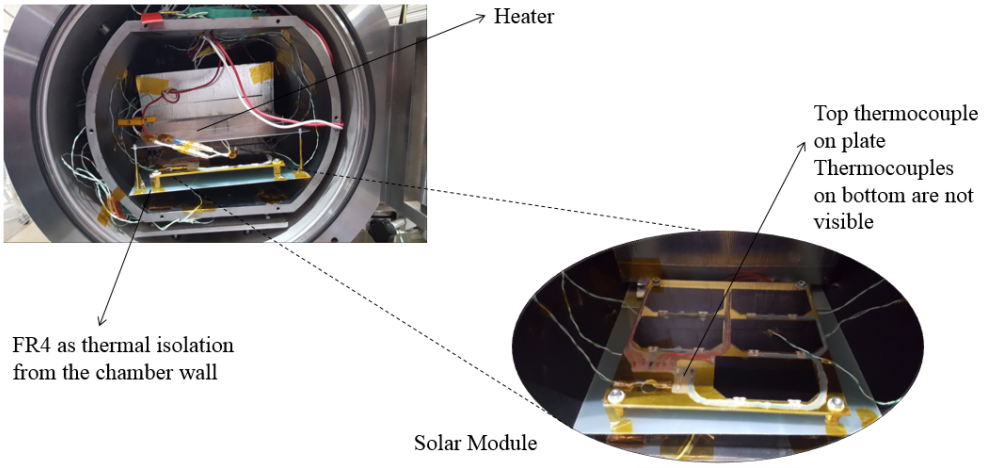

Figure 3.9: Temperature and pressure during TVAC qualification of solar module.

Table 3.6: Durations of hot and cold dwells during Thermal vacuum cycles.

Cycle No.	Temperature (°C)	Duration (h)
1	−30	2.5
	45	1.2
2	−30	4.1
	45	2.2
3	−30	1.2
	45	1.2
4	−30	1.3

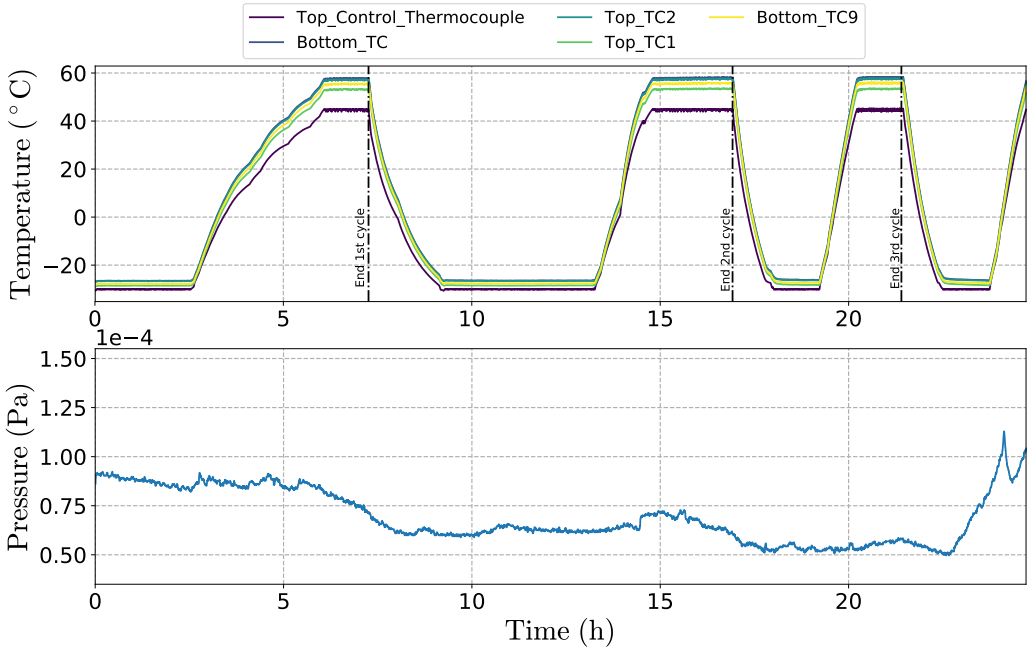

Figure 3.10: Temperatures measured by thermocouples located on the unit obtained during TVAC qualification of SMIC. The pressure in the chamber throughout the test, which was always lower that 1.0×10^{-4} Pa, is also shown.

3.4.3 Experimental Verification

The solar panel was exposed to vibration, shock and TVAC environment described above. The PV curve was measured by using a sun simulator before starting the test sequence, after all vibration tests, after shock and after TVAC tests. The setup that was used to obtain the PV curve for each case is shown in Figure 3.11. There was no change in the performance of the solar panel as shown in Figure 3.12.

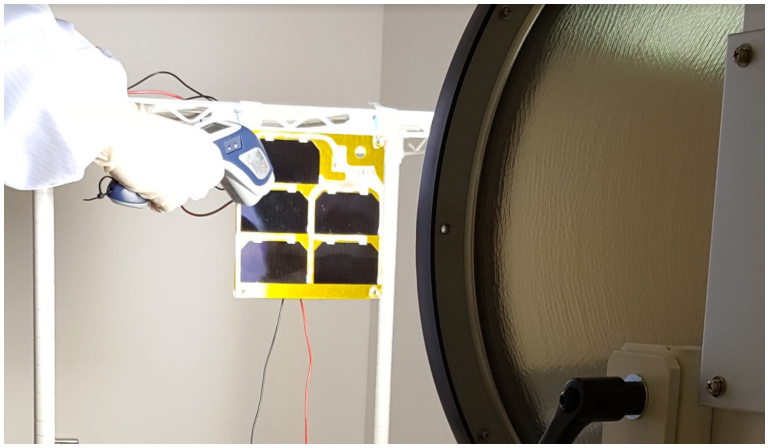

Figure 3.11: SMIC in the sun simulator.

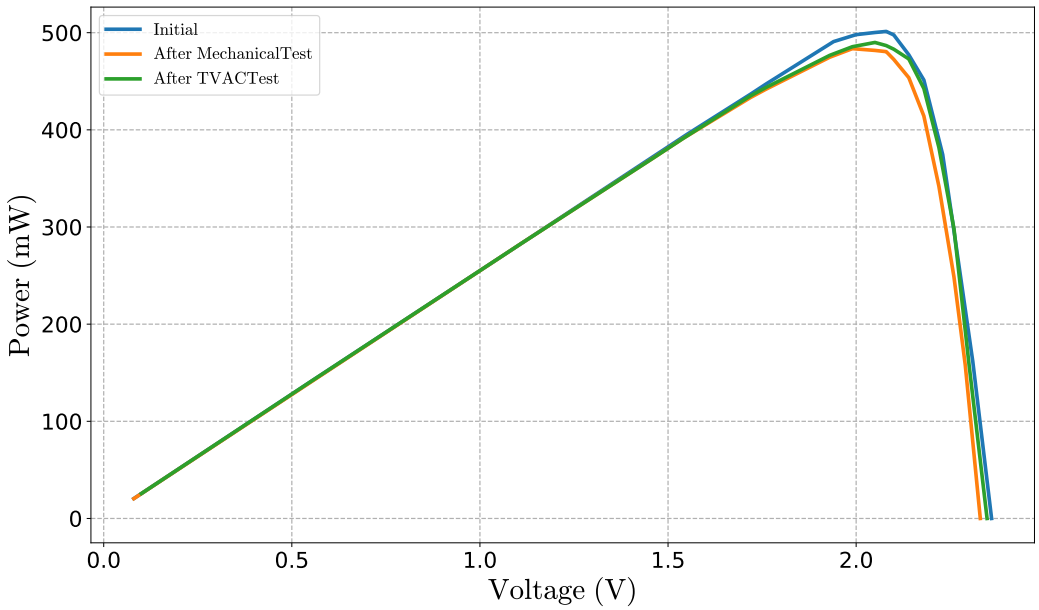

Figure 3.12: Experimental power–voltage (P-V) curve of one solar cell of the module.

Additionally, the SMIC was tested in the sun simulator while charging a flight-representative battery. This test verified that the SAR performed maximum power tracking. Thus, the battery was not fully charged to allow operation at maximum power of the solar array regulator—its open-circuit voltage before the test was 3.796 V. The open circuit voltage and the short circuit current of the solar cell were measured at the irradiance condition of the test: the solar cell open circuit

voltage was 2.39 V, and the short circuit current was 335 mA.

The associated measurements for one solar cell during the test of SAR are listed in Table 3.7. From these measurements, the power obtained by the MPPT from the solar cell can be calculated as $P_{MPPT} = 560$ mW. Using the open circuit voltage, the short circuit current and the manufacturer data, the PV curve was estimated [54, 55], as shown in Figure 3.13, where the maximum power point is indicated as P_{max}. Then, tracker efficiency of the MPPT (TE_{MPPT}) was calculated as

$$TE_{MPPT} = \frac{P_{MPPT}}{P_{max}} \times 100 = 96\%. \tag{3.5}$$

The tracker efficiency indicates the performance of the MPPT. It is also known as Tracking Factor and is usually between 0.86% and 0.99% according to the method used [56, 57]. Thus, the TE of SMIC is in the expected range.

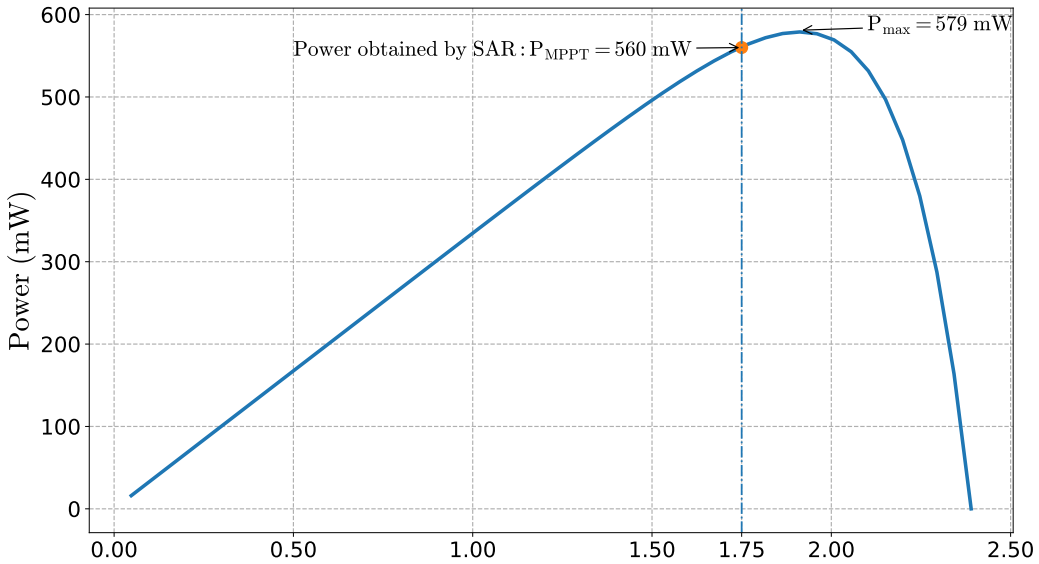

Figure 3.13: Evaluation of MPPT performance by comparison the power obtained and the maximum available power.

Moreover, the efficiency of the SAR dc-dc converter (η_{conv}) can be calculated as

$$\eta_{conv} = \frac{Battery_{current} \cdot Battery_{voltage}}{Solarcell_{current} \cdot solarcell_{voltage}} = 88.49\%. \tag{3.6}$$

Note that this is the efficiency of the dc-dc converter and it is different from the tracker efficiency of the MPPT. The converter efficiency obtained is in the normal range for this kind of dc-dc converter, which is between 80% and 96%. However, higher efficiency of the converter can be obtained by analysis of the power converter [58].

Table 3.7: Measurement during test of SAR as MPPT.

$\boldsymbol{Solarcell_{current}}$ **(A)**	$\boldsymbol{Solarcell_{voltage}}$ **(V)**	$\boldsymbol{Battery_{current}}$ **(A)**	$\boldsymbol{Battery_{voltage}}$ **(V)**
0.3215	1.75	0.127	3.92

3.5 On-Orbit Results of Twelve SMIC

Figure 3.14 presents the time series of Ten-Koh battery voltage and the battery charge currents—two identical batteries have been connected in parallel for redundancy purposes. Negative current has been defined as charging the battery. Since both batteries have been connected in parallel, the combined current for both is the sum of the two currents. Despite the parallel connection, the two currents are consistently different, which is analyzed in more detail below in this section.

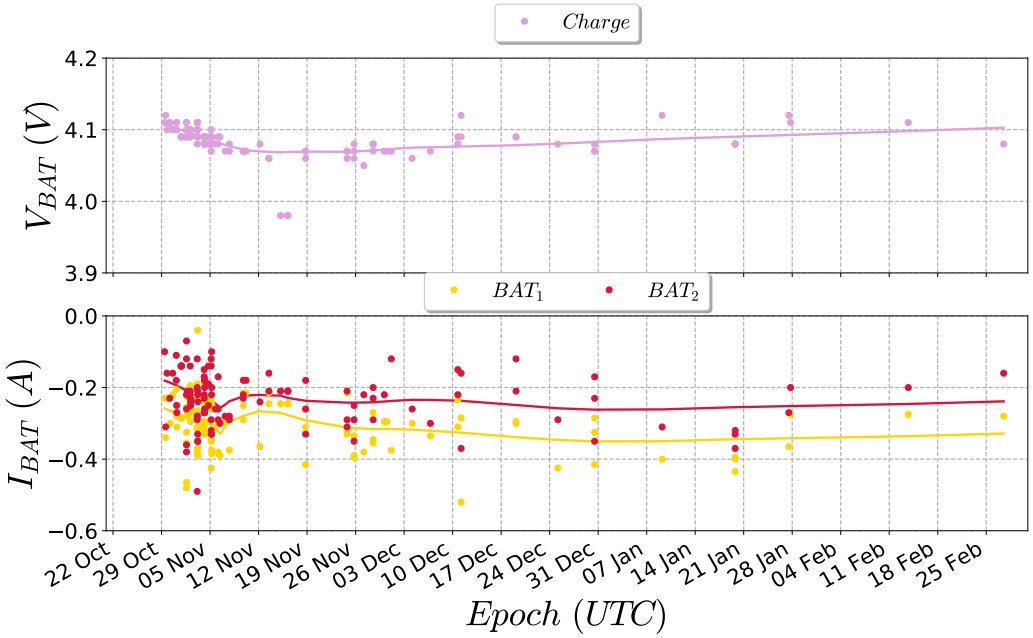

Figure 3.14: Time series of the battery voltage and the charge currents of both Ten-Koh batteries recorded since the launch. The LOWESS regression through the time series is also shown. Negative current has been defined to be charging the battery.

The first observation to be made is that the battery retained its voltage for a duration of nearly five months of spacecraft operations, meaning that the SMICs remained functional and were able to charge the battery and supply power to the spacecraft loads. The data in Figure 3.14 were obtained from the spacecraft beacons transmitted while it was in view of a ground station. Thus, the data become increasingly more scarce after launch, as the radio-amateur community stopped frequently tracking the satellite over time. This fact notwithstanding, the spacecraft remained operational and the battery was charged, meaning that the SMICs were able to supply power to the satellite.

As shown in Figure 3.15, the SMICs were able to provide up to 0.89 A of battery charge current (mean charge current was 0.54 A, and the median was 0.52 A). Note that Figure 3.15 is a cumulative histogram showing the fraction of all measurements that saw a current greater than the corresponding X-axis value. For example, 50% of all measurements had a current greater than −0.52 A.

Figure 3.16 shows the total power generated by the SMICs and the battery voltage over the duration of one orbit. The measurements were taken and stored in satellite on-board memory at an interval of 90 seconds, and later downlinked to ground. In addition to the battery charge current, the spacecraft consumption in sunlight was expected to be 3.3 W. The SMICs were able to provide instantaneous power between 4.35 and 6.68 W during this orbit (up to 0.47 A in sunlight and 0.45 A in eclipse). In addition, it can be noted that the battery voltage was varying according to whether power was being provided to it by the SMIC or not. This means that the SMICs were charging the battery in sunlight, i.e., between Minutes 14 and 75 of the orbit. At that time, the SMIC power output was varying depending on the attitude of the spacecraft.

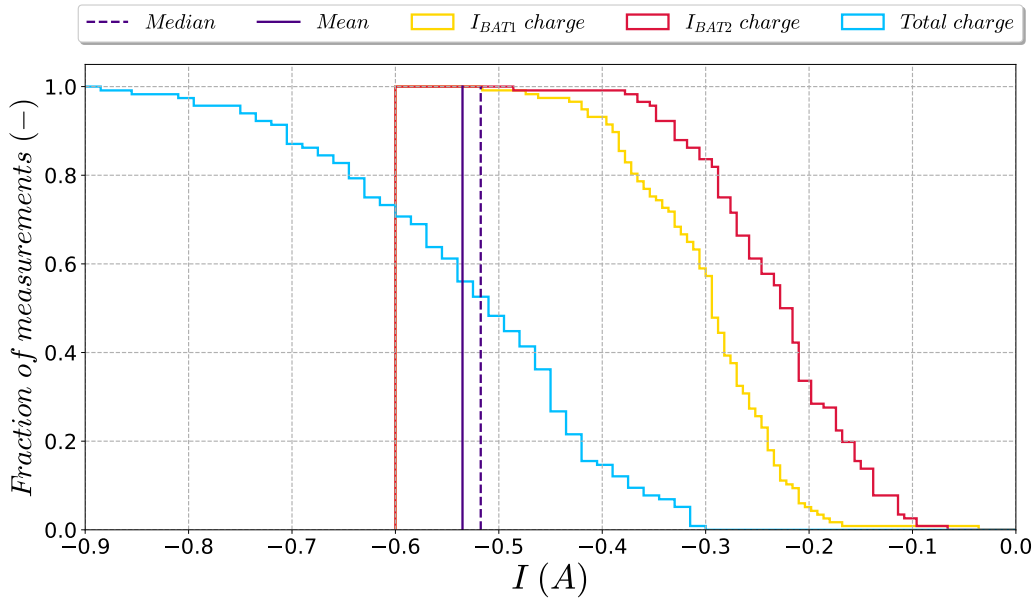

Figure 3.15: Histogram of the charge currents of both Ten-Koh batteries recorded since the launch. The sum of the two currents, and their mean and median are also shown. Negative current has been defined to be charging the battery. Y-axis reports the fraction of all measurements that saw a current greater than the corresponding X-axis value.

The difference between the currents of both batteries over the same orbit as in Figure 3.16 is shown in Figure 3.17. The telemetry of the two batteries is consistently different even though they are connected in parallel and should theoretically

discharge and be charged with the same currents. The same behavior was observed when analyzing data from Figure 3.14. The difference in the current of the two batteries is larger during the sunlit part of the orbit (between Minutes 14 and 75 in Figure 3.17) than in eclipse. However, the difference between the two currents was at most 0.132 A during charging and 0.059 A during the eclipse. This is an order of magnitude less than the measured currents and, therefore, does not affect the results of the above discussion. The difference between both battery currents (Figure 3.17) could be caused by an imbalance of the batteries or inaccuracy of the telemetries. The latter is most probable because the difference is higher during the sunlit that during the eclipse, this means the measuring circuit of battery current 1 (BAT_2) has a higher gain than the measuring circuit of battery current 1 (BAT_1) during the charging process. Based on the orbits results of one orbit and telemetry received by radio amateurs, Figures 3.14 and 3.17 show SMICs providing the power during the sunlit keeping the batteries charged for the operation during the eclipse. This is also a confirmation that SMICs withstand the launch environment and about five months in LEO, more than 1500 orbits.

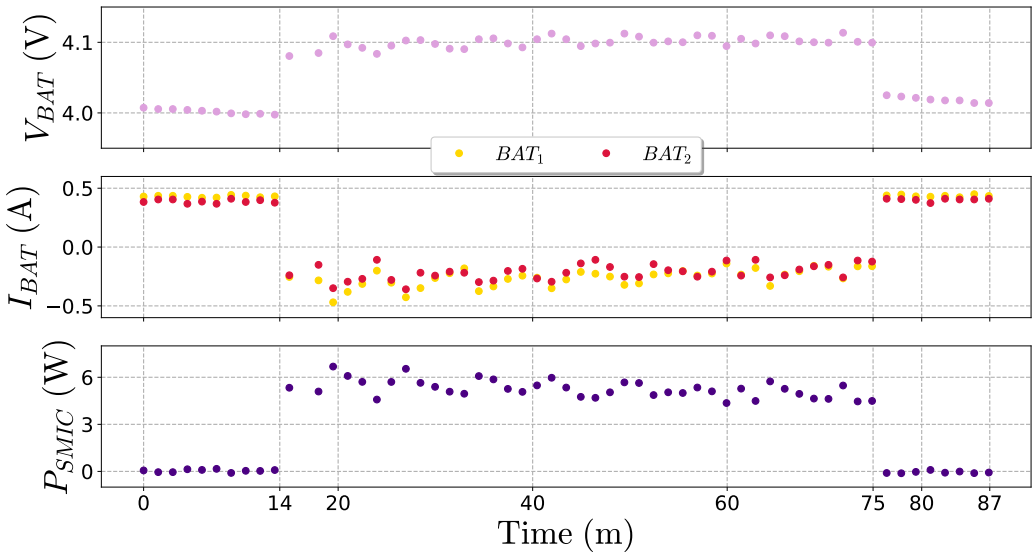

Figure 3.16: Battery voltage (V_{BAT}), battery current (I_{BAT}) and total generated power by the SMICs (P_{SMIC}) during one orbit.

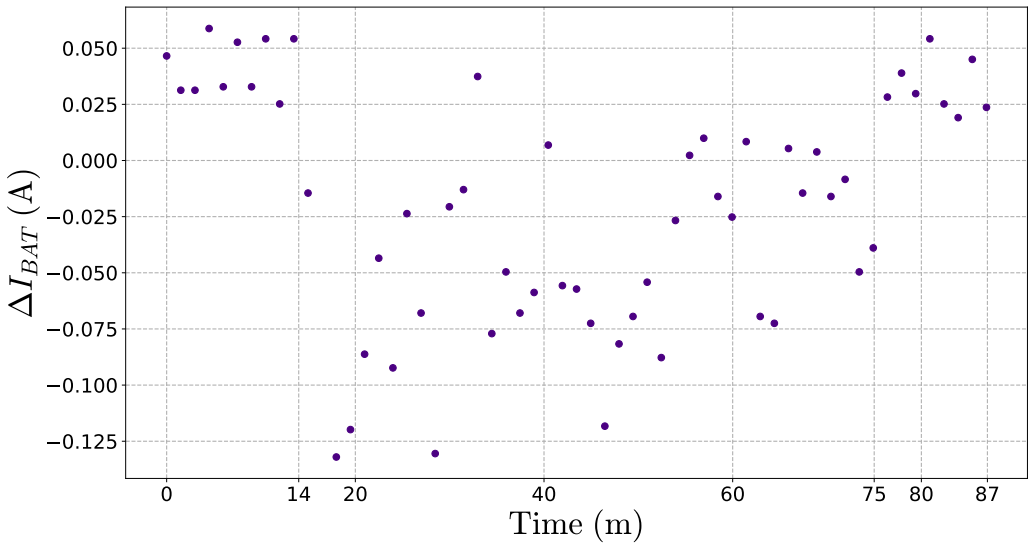

Figure 3.17: Time series of the difference between currents of batteries 1 and 2 ($\Delta I_{BAT} = I_{BAT1} - I_{BAT2}$) during one orbit. Negative current has been defined to be charging the battery.

3.6 Summary

A modular approach for the power generation component of small satellites, called Solar Module Integrated Converter is presented. The general architecture of the SMIC, design considerations and evaluation approach are proposed and detailed. Moreover, the proposed SMIC architecture and method to the design of solar array is applied to Ten-Koh satellite. The modular approach allows the inclusion of multiple functional requirements in one module such as power generation, solar array regulator and measurements required for housekeeping.

Chapter 4

Results of EPS in small spacecrafts: Ten-Koh case

Small satellites have especial applications for education, technology demonstration and space science[59]. This is the case of Ten-Koh satellite; a small satellite of 21 kg for monitoring the LEO environment. This satellite, developed in Kyushu Institute of Technology in 1.5 years, was launched on October 29th on board HII-A No. 40 rocket. This chapter describes the EPS designed for Ten-Koh satellite, which is a hybrid EPS that combines centralized and distributed architecture to take advantages of the Solar Module Integrated Converter (SMIC) described in the previous chapter [9]. In addition, this chapter presents the architecture and main components and it also analyzes the in-orbit results of the designed EPS.

4.1 Introduction

The design of the electrical power system of is one of the main challenges of the small satellite development and it is recommended to follow a simple approach [16]. Ten-Koh satellite (Fig. 4.1) has a quasi-spherical shape with no attitude control that uses the same shape of Shinen 2 [21, 60]. Thus there is no specific orientation for the solar panels. The orbit of satellite determine the solar irradiance and the

duration of eclipse and sunlit periods. Tenkoh satellite was launched as piggyback of GOSAT-2, thus it follows a sun-synchronous sub-recurrent orbit with an altitude, h, of 613 km and an orbital period of 5817.45 s. The initial parameters of the orbit are detailed in Table 4.1.

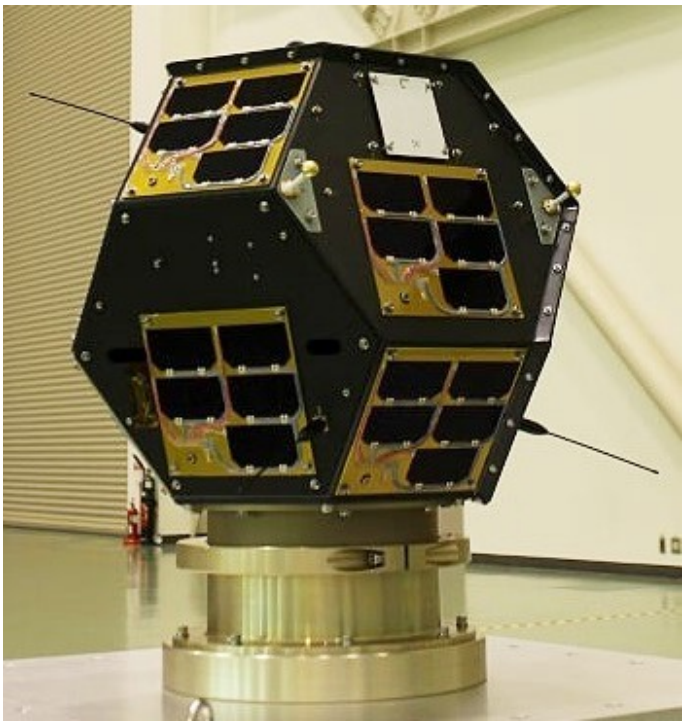

Figure 4.1: Flight model of Ten-Koh satellite.

Table 4.1: Parameters of Ten-Koh initial orbit

Parameter	Values
Inclination	97.835
RAAN	4.6815
Argument of perigee	27.546
Semimajor-axis	6969.772
True anomaly	212.990
Eccentricity	0.002586

The EPS must provide the power to itself and all the spacecraft subsystems[18]. In the case of Ten-Koh, the main components are the On-board computer (OBC), two redundant communications subsystems (COM-1 and COM-2), the Attitude determination subsystem (ADS) and the payload components (Experiment Control Unit (ECU), Double Langmuir probe (DLP), Charge particle detector (CPD) and

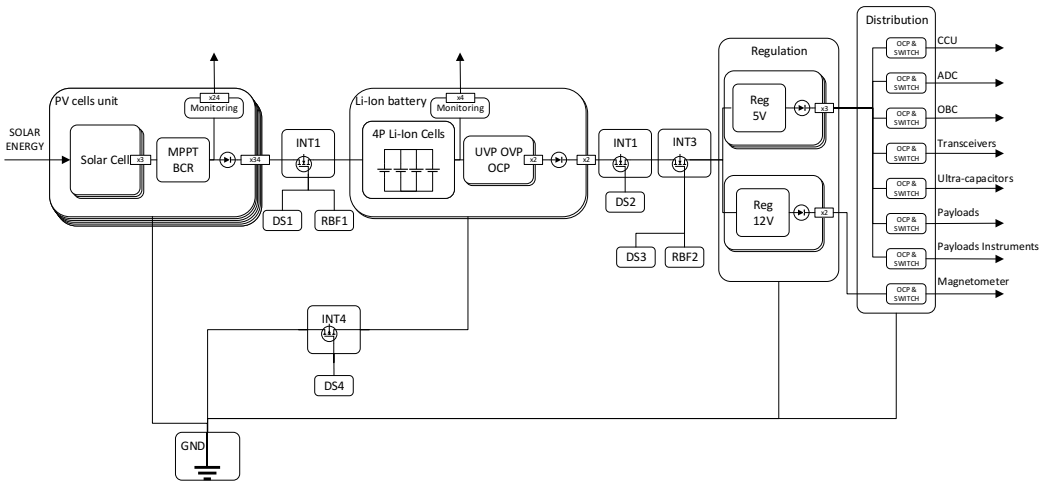

Figure 4.2: Architecture of Ten-Koh EPS

secondary payloads). Table 4.2 shows the required voltage and the maximum allowed current.

Table 4.2: Power consumption of Ten-Koh subsystems.

Subsystem	Voltage (V)	Peak current (A)
OBC	5.0	0.70
COM-1	5.0	1.35
COM-2	5.0	1.35
ADS	12.0	0.70
EPS	5.0	0.70
ECU	5.0	1.35
DLP	5.0	1.35
CPD	12.0	2.00
PL-2	5.0	2.0

The architecture of the EPS of Ten-Koh is shown in Fig. 4.2. The power generation is based on triple junction solar cells as energy source that are assembled in 12 solar modules. As energy storage, two hot-redundant battery packages are used. As power regulation, dc-dc converters are used to generate the two main power lines and there is a test results as well as on-orbit data of electrical power systems are included for every subsystem.

The satellite uses body mounted solar cells to obtain the energy required by the satellite bus and the payloads. Thus, only the cells located in the sunlit side can

generate power; however, most of the surface has to be covered because the satellite spins in all axes. The detail of Ten-Koh solar array is described in Section 4.2.1

To keep operation during the eclipse time, Ten-Koh uses batteries as energy storage. Lithium-Ion battery cells were selected based on their flight heritage. The description of the array of battery cells is described in Section 4.2.2

The solar array output control, the battery charge control and the battery discharge control are implemented using COTS components with flight heritage. Maximum power point tracker technique is used as solar array regulator, interfacing the solar panels with the main bus. This power architecture is known as battery-clamped bus peak power tracking. Additionally an independent device is responsible for battery protection. The details are presented in Section 4.3. This section also describes what kind of inhibits are used to meet the safety requirement and keep the satellite off during launching.

Most of the payloads require a regulated voltage of 5 V or 12 V. Switching converters are used to obtain the regulation from the battery bus. Details of this converters are explained in Section 4.4

Measurements of EPS performance have been received since launching during 5 months. The received data confirms that EPS met the requirement providing the power to the spacecraft during nominal mode and during the missions. House keeping data is presented in Section 4.5

4.2 Power Source and Energy Storage

As energy source, Ten-Koh uses triple junction solar cells and lithium-Ion battery cells as many other satellites[61]. However, Ten-Koh EPS uses an specific design to meet the spacecraft requirements. Below, it is detailed the solar array and the battery packages.

4.2.1 Solar Array

The solar module consists of five triple junction solar cells being able to generate up to 5 W at BOL when operating at maximum power. The specifications of the solar cell are listed in Table 4.3[51]. Each cell can generate 1.0 W at Standard Test Condition (STC).

Table 4.3: Electric specification of Solar cell at AM0 (1367 W/m^2), 25° C.

Parameter	Values
Open circuit voltage, V_{oc}	2.6 (V)
Voltage at maximum powet, V_{mp}	2.32 (V)
Short circuit current, I_{sc}	473 (mA)
Current at maximum power, I_{mp}	455 (mA)

The five cells are configured in two arrays because the solar array regulator that was selected can handle a maximum 3 W (Section 4.3.1). Thus, one array consist of three cells connected in parallel and the other of two cells connected in parallel.

Each array include a solar array regulator to extract the maximum power of the array, which also can limit the output voltage to avoid overcharging the battery as explained in next section. All the arrays are connected in parallel to supply the power into the battery bus.

4.2.2 Batteries

Li-Ion electrochemical cells have been used for small satellites due to their high specific energy [62]. Ten-Koh satellite uses COTS li-Ion cells following the heritage of Shinen-2 and many other small satellites and CubeSats [36].

Ten-Koh uses two identical battery packages to implement redundancy.Each battery package consists of four Li-Ion cells connected in parallel with a nominal capacity of 46 Wh. This determines the bus voltage can vary from 2.8 V (discharged) to 4.2 V (charged). Each battery package includes independent protection circuit

against overvoltage, overcurrent and undervoltage and short circuit as described in Section 4.3.1.

Table 4.4: Specification of Lithium-Ion battery cell NCR18650B

Parameter	Values
Rated capacity	3200 (mAh)
Nominal voltage	3.6 (V)
Voltage (charged)	4.30 (V)
voltage (discharged)	2.5 (V)
Mass	48.5 (g)
Temperature (Charge)	0 to 45 °C
Temperature (Discharge)	-20 to 60 °C

4.3 Power Control Unit

Solar arrays and batteries require different kind of power control. The battery requires charge and discharge regulator to keep the voltage and current among safe range. The solar array power is controlled to extract the maximum or to limit when it is not necessary. In addition, both solar array and batteries can not provide a regulated voltage, thus a voltage regulator is also necessary to provide the voltage required by each subsystem. This section explain how these power control module were designed in Ten-Koh EPS.

4.3.1 Battey Charge and Discharge Control

Each solar array of three cells and two cells is connected to one battery charger regulator and solar array regulator (MPPT IC SPV1040). This IC was selected as legacy of Shinen-2 deep space probe [63]. This IC maximize the power delivered by the solar array by using MPPT algorithm or regulate the voltage when the battery is fully charged; its specifications are shown in Table 4.5. This IC is a step-up converter, thus the output voltage should be greater than the input,in Ten-Koh case the solar array voltage is near to 2.32 V and the output voltage is between 2.8 and 4.2 V.

Table 4.5: Electric specification of battery charge with MPPT SPV1040

Parameter	Values
Input voltage range	0.3 to 5.5 (V)
Output voltage range	2 to 5.2 (V)
Maximum output power	3 (W)
Temperature	-40 to 155 (°C)

Battery protection from overcharge, overdischarge and over current is also included. This protection is implemented with IC S-8261, which monitors the battery voltage and current to detects the abnormal conditions. External MOSFETs are required for disconnecting the battery when the detected battery voltage is outside of the specified range (Table 4.6).

Table 4.6: Specification of battery protection circuit S-8261

Parameter	Values
Overcharge	4.28 (V)
Overdischarge	2.80 (V)
Overcurrent	5.00 (A)

4.3.2 Power deactivation switches

The inhibit scheme shall ensure that the satellite is completely powered off during launch, this means no power is given to the payloads and no power is given to or taken from the batteries. Several of the possible hazards are related to the battery, there are three main sources of hazard in Li-Ion batteries (JSC-20793 Rev D. p61): overcharge; internal and external short; high temperatures; and overdischarge. Some of these hazards cannot be prevented using the inhibits scheme, like the high temperatures which can be prevented with a good thermal design; and the internal shorts that are prevented by screening the cells from defects.

The hazards that are prevented with the inhibit scheme are: (1) overcharge; (2) external short; (3) overdischarge; and (4) accidentally turning on the payload. In the case of Ten-Koh, the design of the inhibits was developed to be two fault tolerant as shown in Table 4.7 and Figure 4.3.

Table 4.7: Inhibit scheme

Hazard	INH 1	INH 2	INH 3
Overcharge	SW1a	SW1b	PSW
External short	SW1b	CID	PSW
Overdischarge	SW2	SW3	PSW
Payload power on	SW1	SW2	SW3

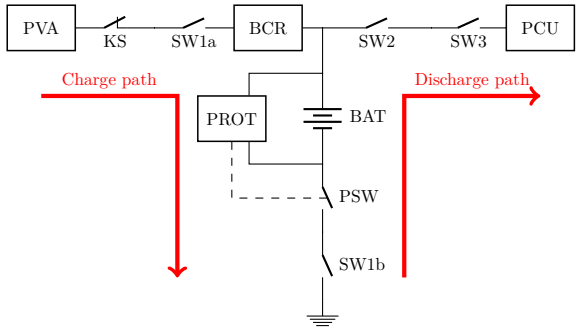

Code	Detail
PVA	Photovoltaic array
PCU	Power control unit
BAT	Li-Ion Battery
PROT	Protection IC for Li-Ion
KS	Kill switch
PSW	Protection switch
CID	Current interruptive device
PBF	Put before flight screw
DSW	Deployment switch
SW1	DPST Switch, activated by PBF1 and DSW1
SW2	SPST Switch, activated by PBF2 and DSW2
SW3	SPST Switch, activated by PBF3 and DSW3

Figure 4.3: Inhibit schematic

4.4 Power Regulation and Distribution

As described before, the battery bus oscillates between 2.8 and 4.2 according to the state of charge. Therefore, a voltage regulator is required to provide a safe voltage to each subsystem. This voltage regulator is based on dc-dc converter, LT1370, which is a current mode switching regulator that allows parallel connection to implement hot-redundancy.

To implement overcurrent protection (OCP) for every subsystem, one Overvoltage overcurrent protection Controller (LTC4361) is installed in each power line. This is set up to limit the current according to limit specified in Table 4.2.

Even though the EPS is based on centralized power regulators, some subsystems

require specific regulators. For example, ADS system is powered from 12 V power line because it is the requirement for the magnetometer. However, it uses specific regulators to generate 3.3 V. This is used for SD card memory, Gyros and the level shifters. Additionally, 5.0 V is required for the analog to digital converters ADC. This distribution system of the power lines in the ADS are shown in Fig 4.4.

A different case of power distribution is the DLP power board. In addition of the requirement of additional voltage levels (12.0 V, -12.0 V), it is also necessary to have different reference ground. Therefore and isolated dc-dc converter is included to generate the 12.0 V, -12.0V and 5.0V with isolated 0V reference (Fig. 4.5).

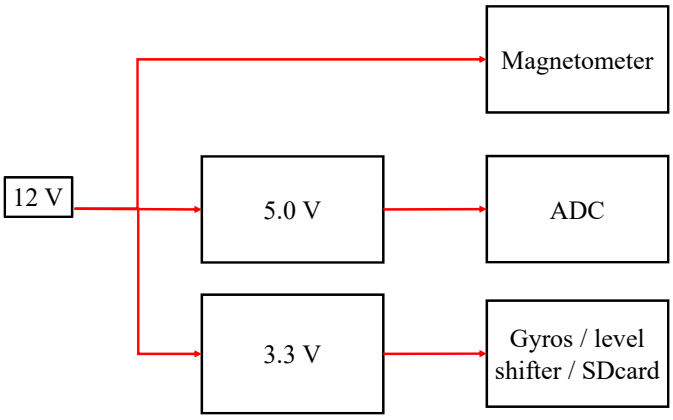

Figure 4.4: Power distribution in ADS systems

4.5 In-orbit results of Ten-Koh EPS

The EPS was designed, implemented and integrated in the Ten-Koh platform. Fig. 4.6 shows the external view and internal view of Ten-Koh spacecraft. Five identical solar panels can be seen in the external, each array with five cells at

different incidence angle. The battery 1 is shown in the internal view, battery 2 that is located in opposite side is not shown.

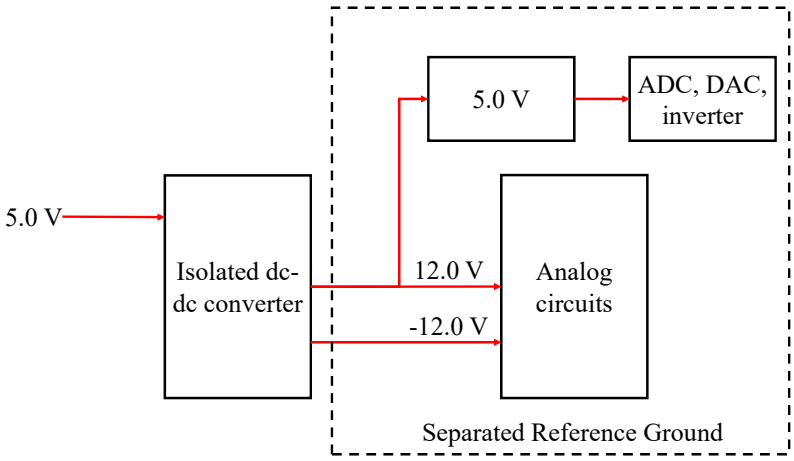

Figure 4.5: Power distribution in DLP systems

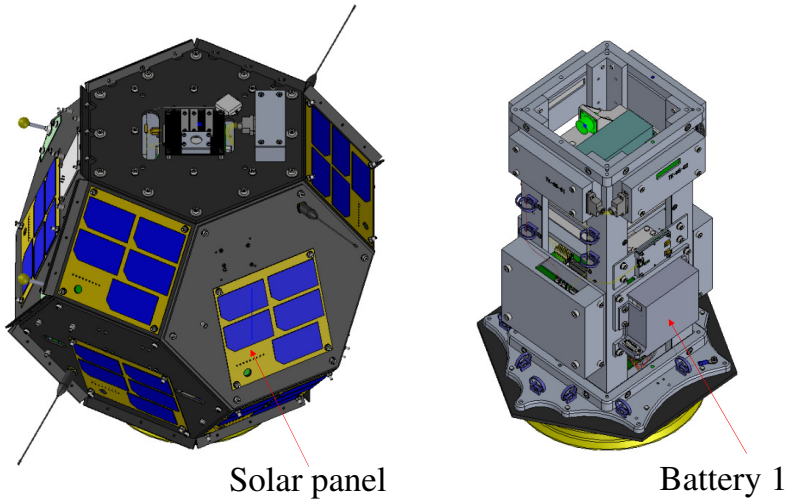

Figure 4.6: Ten-Koh CAD view. External view with solar panels (left). Internal view showing the battery 1, battery is located in the opposite side and it is not shown (right)

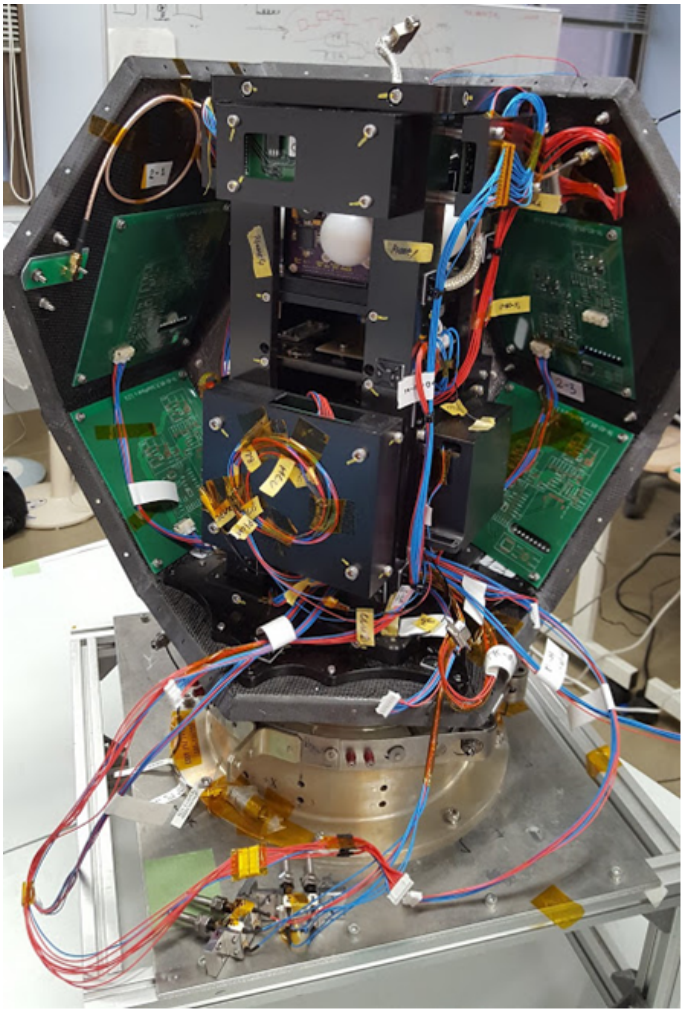

Figure 4.7: Ten-Koh external and internal view

The satellite was launched on 29th October 2018 at 04:08 UTC since Tanegashima Space Center. The separation of rocket was 33 minutes after launching (Fig. 4.8). The beacon was received during the first orbit in Argentina by LU1CGB and in USA by K4KDR.

The received beacon by K4KDR was decoded as JG6YKY:8F5CEE66365F86704168F681N. That includes the measurements of battery voltage, battery current and battery temperature as listed in Table 4.8.

Battery voltage has been monitored since launching. Fig. 4.9 shows history of voltage received in different parts of the world at different times by volunteers

Table 4.8: Ten-Koh housekeeping during first orbit

Parameter	Values
Battery 1 Current	0.37 A (Discharging)
Battery Voltage	4.04 V
Battery 1 Temperature	20.58 °C
Battery 2 Temperature	19.86 °C
Battery 2 Current	0.32 A - (Discharging)

radio amateurs. The top series of data are the voltages when the satellite was receiving sun light; the voltage varies between 4.05 V and 4.12 V. In the same figure the bottom series shows the battery voltages during eclipse; in this case the battery voltage goes from 3.97 V to 4.04 V.

The measurements history of battery-1 (BAT_1) current and battery-2 (BAT_2) current is shown in Fig. 4.10. The battery current is defined as positive when discharging and negative when charging. During eclipse, the two batteries provide around 0.4 A each as seem in the to series. When the batteries are being charging by the solar array, the current in each battery is varying due to the spinning of Ten-Koh. That means the generated power is changing while the orientation of the spacecraft is changing regarding the sun.

The temperature measurements history of both battery packages, which is shown in Fig. 4.11, indicates that the batteries has been always operating in a safe range during the five months of received data. Both temperature measurements are between 10 °C and 21 °C which are in the recommended operating range indicate in Table 4.4. There is a significant difference between the temperature of the two batteries caused by the location of the two batteries, they are located in opposite sides of Ten-Koh internal structure.

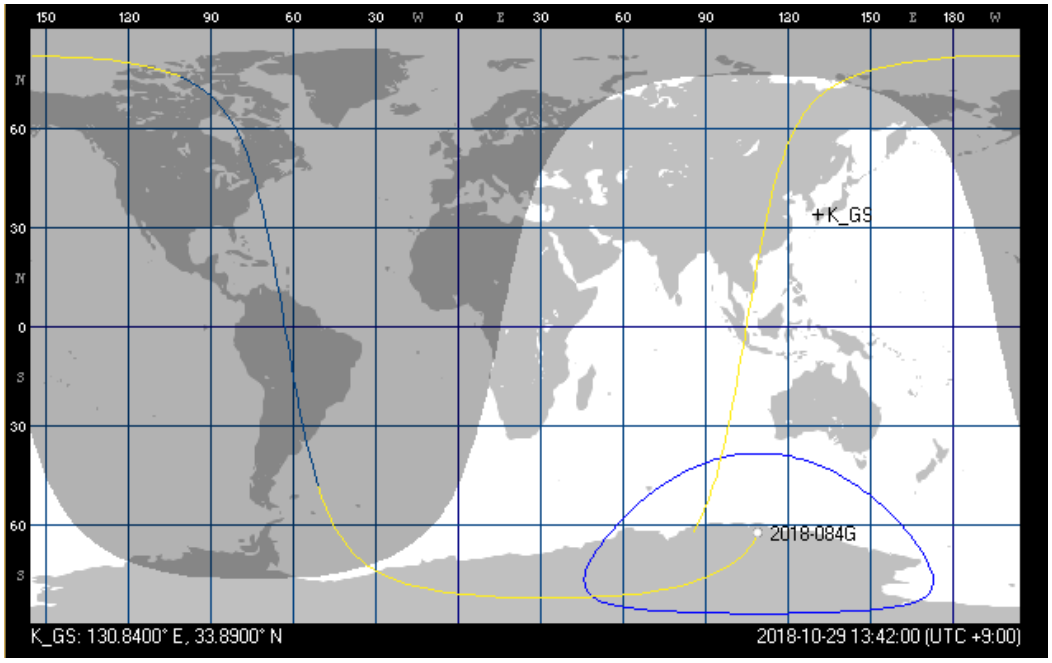

Figure 4.8: Ten-Koh first orbit identified as 2018-084G

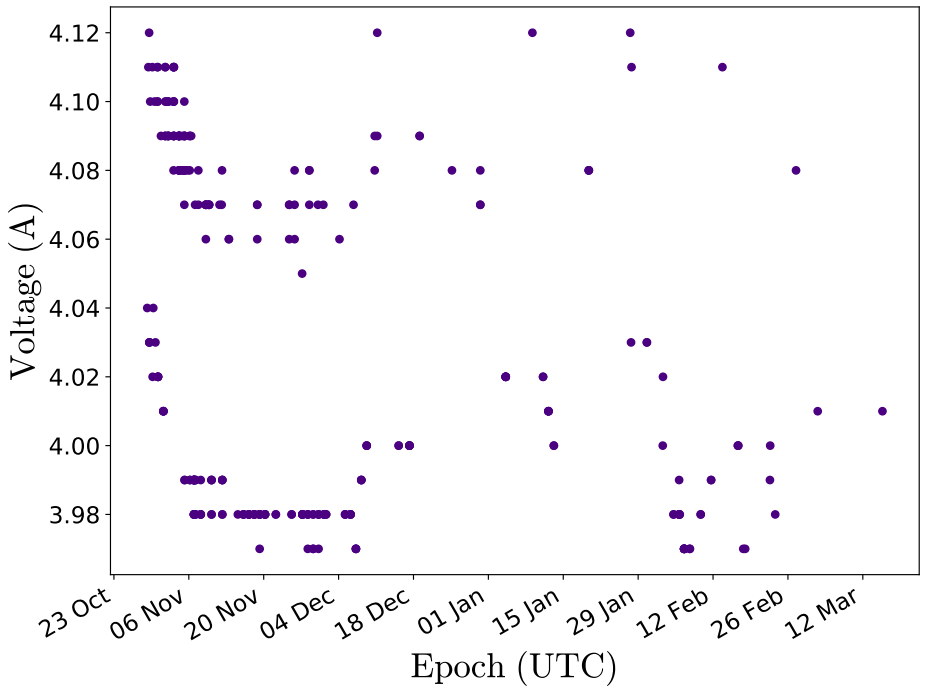

Figure 4.9: History of battery voltage since launching

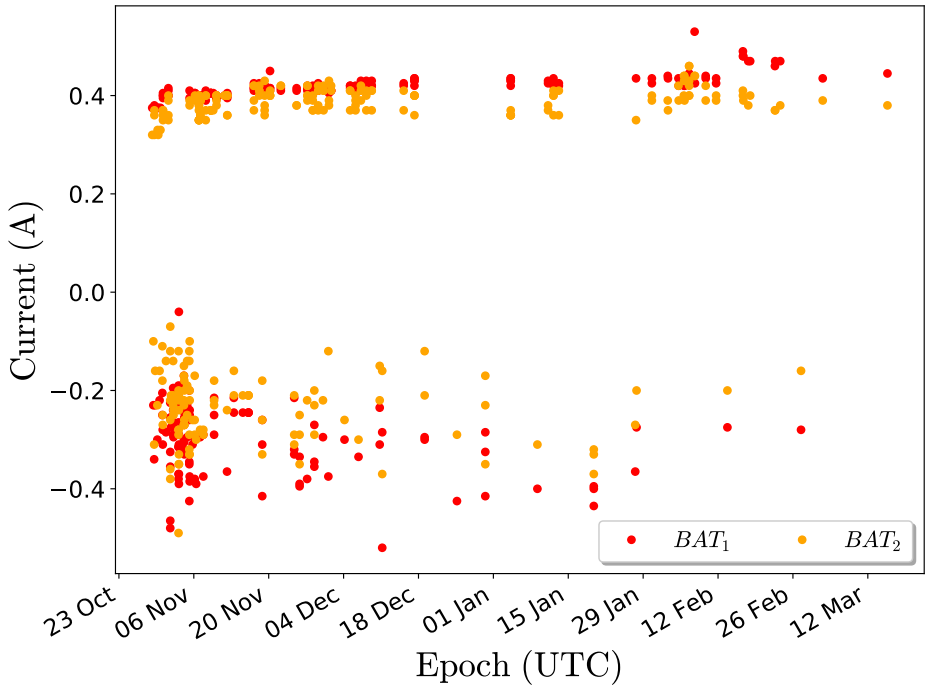

Figure 4.10: History of battery currents since launching

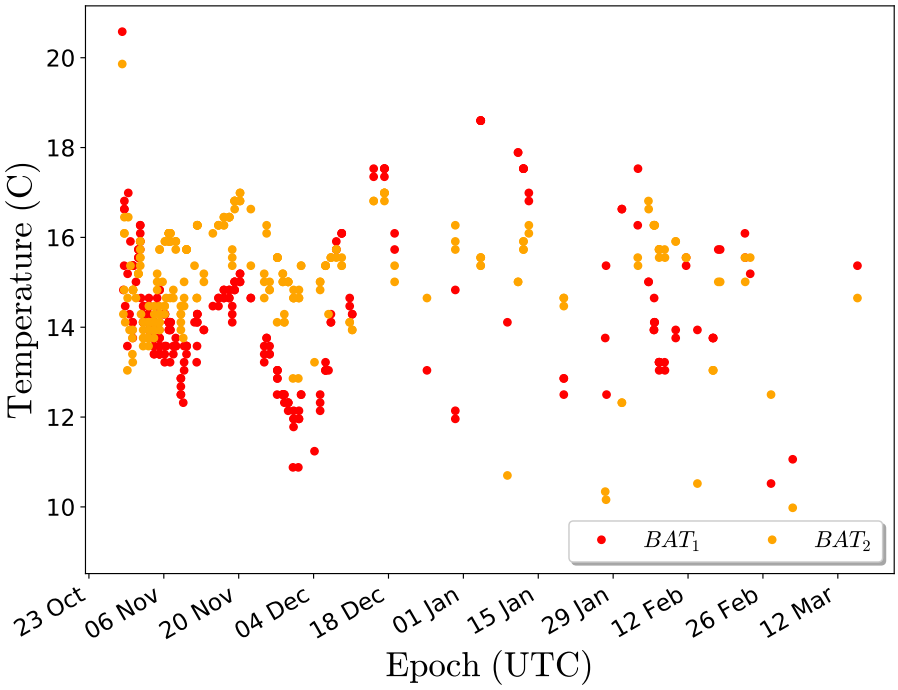

Figure 4.11: History of battery temperature since launching

4.6 Summary

An electrical power system (EPS) was developed for a quasi-spherical satellite in sunsynchronous orbit. The satellite was launched on 29th October of 2018 since Tanegashima Space Center. The housekeeping data was received in the first orbit. The housekeeping data received since launching during 5 months of operation confirms that designed EPS met the power requirement of Ten-Koh satellite. Primary and secondary missions were executed in this period and the data was received in Ground station. The approach used in Ten-Koh EPS allows the validation of redundancy in several level. First, the power generation is based on a solar multi-array that uses 12 identical solar module. Two hot redundant batteries and two dc-dc converter connected in parallel for the regulation of 5 V and 12 V.

Chapter 5

Experimental results of ultracapacitor in Low Earth Orbit on-board Ten-Koh

5.1 Introduction

Supercapacitors interest as energy source in space applications has increased lately due to his longer life cycle and the wider temperature range. In addition, The higher power capability of Supercapacitor compared with typical rechargeable batteries will bring more applications to small satellites by enabling high power demand payloads [64, 65].

One of the main limitations of supercapacitor as main energy storage is their low energy density. However, Supercapacitors can be used as the main energy storage for Cubesats as proposed in [66, 67]. These works provide some suggestions about the electronic parts that can be used to develop such system using ultracapacitors as only energy storage without backup. Considering the limitation, supercapacitors can be used in hybrid systems, where the supercapacitor main advantages of providing high power can be complement to traditional batteries.

Using Component-off-the-shelf (COTS) has allowed the development of small satel-

lites. Thus, the use of COTS supercapacitors that have not been developed for space application is the interest of space community. Therefore, there has existed and interest to confirm if they can be used in space. A qualification test was developed in commercial supercapacitor of Electric Double Layer Capacitor (EDLC) by [68]. It is reported the test results under vacuum, shock, vibration and radiation test vacuum. Recently, thermal vacuum test of commercial supercapacitor has been reported by [69]. These test have reported that the COTS supercapacitor evaluated withstood the environment conditions without thermal o mechanical protection.

5.2 Experiment

An commercially available supercapacitor was selected to be tested in LEO orbit. The supercapacitor was integrated into the spacecraft into a experiment board that charge and discharge the supercapacitor while record voltage, current and temperature. After spacecraft started the mission mode, the supercapacitor was charged and discharged during the passes over the Ground Station, receiving the measurements in real time. This section details the material and methods during the supercapacitor test in LEO orbit.

5.2.1 Supercapacitor selection

An Electric Double Layer Capacitor was selected among the commercially available components. The capacitor was selected considering both the size and the capacity. The size was a restriction due to the volume and mass available in the spacecraft. The energy capacity was a key parameter considering that the it can be used in a mission as proposed in [66]. One COTS supercapacitor of 400 F was selected, its specifications are listed in Table 5.1.

Parameter	Value	unit
Capacitance	400	F
Working voltage	2.70	V
Surge voltage	2.85	V
Operating temperature range	-40 to 65	°C

Table 5.1: Specifications of the supercapacitor

5.2.2 Design of experiment board

A circuit to charge and discharge the supercapacitor was designed and implemented to do a cycle of the ultracapacitor on board the spacecraft. This system, described in Fig. 5.1, has two discharging path: 1) constant resistor, and 2) into the power bus to recover the energy. Thus the discharging mode is not possible at constant current. The option to discharge into the power bus allows to recover part of the energy that is not dissipated by the the boots converter that connects the supercapacitor to the power bus.

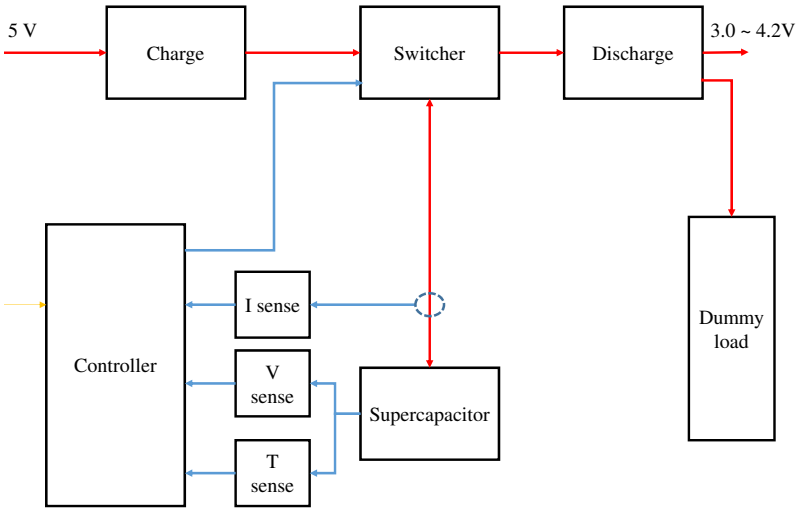

Figure 5.1: Components of the charger and discharger experiment

The supercapacitor charger circuit is powered from the constant voltage input (5.0 V) provided by the electric power system of the spacecraft. To safely charging,

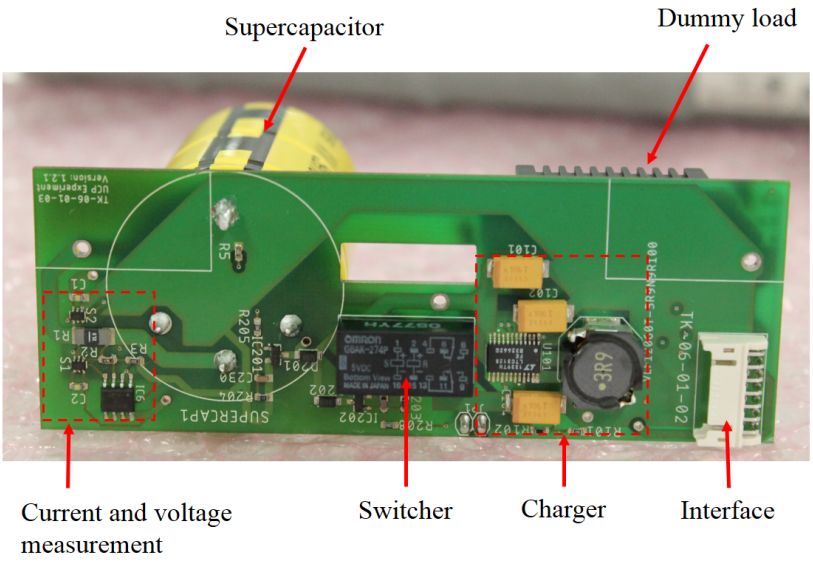

Figure 5.2: Implemented experiment board

input current limit of 1.0 A and maximum voltage charge of 2.74 V were set up in the charger. This is implemented with monolithic buck-boost converter LTC3128 that is commercially available. In addition, it has a shutdown input to disable the charger when the experiment is off.

The experiment board includes two options to discharge the supercapacitor: First, a wire wound high power resistor of 1.0 Ω and maximum power rate of 10 W. Second, a boots converter to step up the voltage to the battery bus (3.0 to 4.2 V); however, this option does not allow to control the current output and it is implemented to avoid waste of energy when required by the spacecraft. The implemented board in shown in Fig. 5.2

The circuit is controlled by a microcontroller to start/stop the experiment in charging or discharging mode. The microcontroller also record the voltage, the temperature and the charging or discharging current. The mode is commanded by a communication interface through I2C to be able to program the operation according to the mission plan considering the energy status of the satellite. Basically, the controller can start in three modes: charging, discharging and disable. This controller is implemented with a PIC16F877 because it has flight heritage to operate

in LEO in previous small satellites without much problem due to space radiation.

The voltage of the UCP is measured very close to the terminals using the internal 10 bits ADC and conditioning circuit to adjust the voltage measurement to the maximum level of the ADC (2.5V). The current measurement is implemented with one shunt resistor of 2 mΩ that is shared by two current-shunt monitors sensing opposite polarities; in this was, charging current and discharging current are measured in the full scale of the ADC. This is each current-shunt monitor amplifies the voltage of the shunt resistor and it is connected to ADC.

One temperature transducer is installed on the bottom of supercapacitor. The transducer has contact with the base of the supercapacitor and it produces an output current proportional to the temperature. This output is connecte to current to voltage conversino resistor and read by the ADC. The temperature range of the transducer is from -55°C to 150°.

5.2.3 Experiment Integration in the spacecraft

The UCP experiment board is integrated into the spacecraft as shown in Fig. 5.3. It is located in the internal structure where the main electronic boards of the spacecraft bus are located. Below the UCP experimental are located the PCB of the On-Board Computer, the Electric Power Supply Controller, the Communication Controller. Thus, the UCP temperature is expected in the same range of the spacecraft bus.

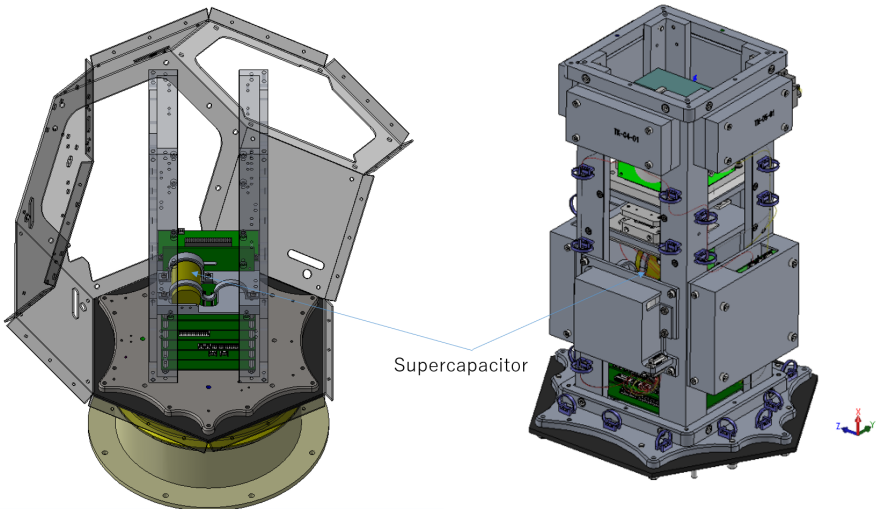

Figure 5.3: Location of UCP experiment board in the spacecraft in the CAD model.

When the all the components are integrated is visual blocked by aluminum boxes that installed on the main internal structure (Fig. 5.4). These aluminum boxes contain the regulator board of the electrical powet systems and the battery.

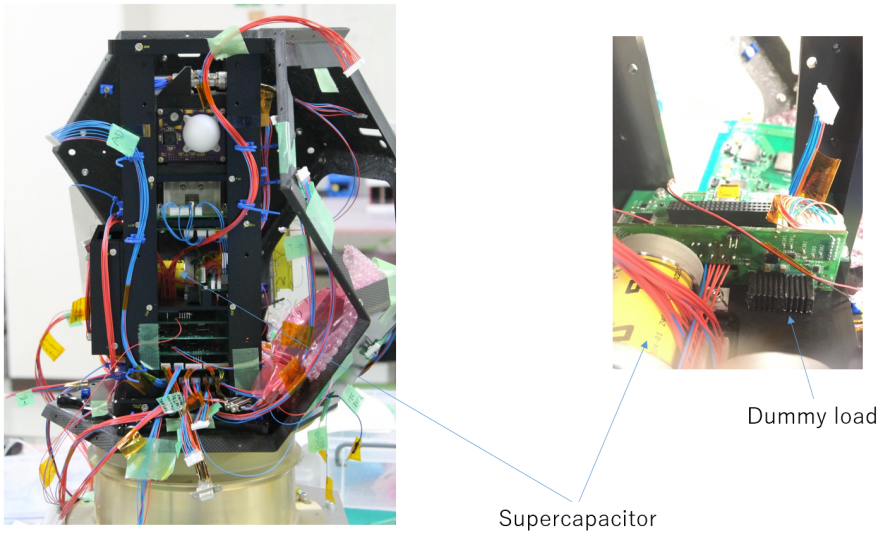

Figure 5.4: Location of UCP experiment board in the spacecraft in the Flight model.

5.2.4 Test during orbit operation

The UCP experiment board was operated only during passes over GS which has a duration of 12 minutes. Thus, several passes were required to complete one charge/discharge cycle. The operation included to read the voltage, temperature, charge current and discharge current; then to start charge or discharge according to the sequence. The UCP started discharged, thus, the first goal was to charge it until 2.7 V and later discharged until 1.4 V to complete the first cycle in orbit.

Before the pass finish, the experiment was stopped to continue the charge-discharge cycle only in real time. The measurements were received in the ground station. In addition to complete the charge-discharge cycle, this mode of operation allowed the observation of self-discharge because the time between operation was varying form 12 hours until several weeks. Nex section will present the results of the experiment during almost five months in LEO orbit.

5.3 Results and discussion

The minimum success criteria of achieving at least one cycle was achieved (Fig.5.5)This can confirm that the UCP withstand the mechanical stress of the acceptance test of the spacecraft, the launch environment of H-IIA rocket as piggyback and LEO environment after XXX orbits. Fig. 5.5 shows the UCP voltage (V_UCP) from 0.5 V until 2.7 V during charging and from 2.7 V to 1.4 during discharging (Blue continues line). The constant voltage indicates that measurements were taken when no charging or discharging were executed.

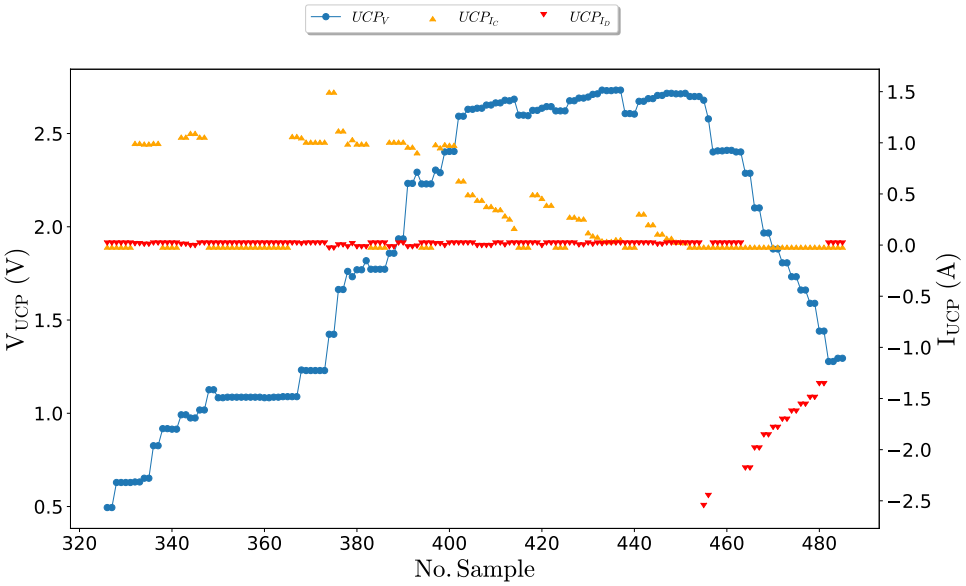

Figure 5.5: One cycle charging and discharging the UCP.

The UCP charge current (UCP_{I_C}) and UCP discharge current (UCP_{I_D}) are also shown in Fig. 5.5. Negative values indicate that UCP is discharging. The charging current is around 1.0 A while charging and the UCP_V is below 2.5 V, above this value the charging current decreases while the UCP_V achieve the nominal voltage of 2.7 V. This behavior indicates that the charger is not forcing the constant current mode.

Three cycles were completed until communication with the spacecraft fail after five months in orbit taking 485 packets. Fig. 5.6 and Fig. 5.7 show the ultracapacitor measurements history: voltage (V_{UCP}), charge current (I_{charge}), discharge current ($I_{discharge}$) and temperature (T_{UCP}). The first cycle was executed in two months, the second cycle in two weeks and the last cycle in one week. It is observed that that ultracapacitor was operating in different temperature ranges from 6 to 22 $°C$. There are measurements only during the passes over the ground station.

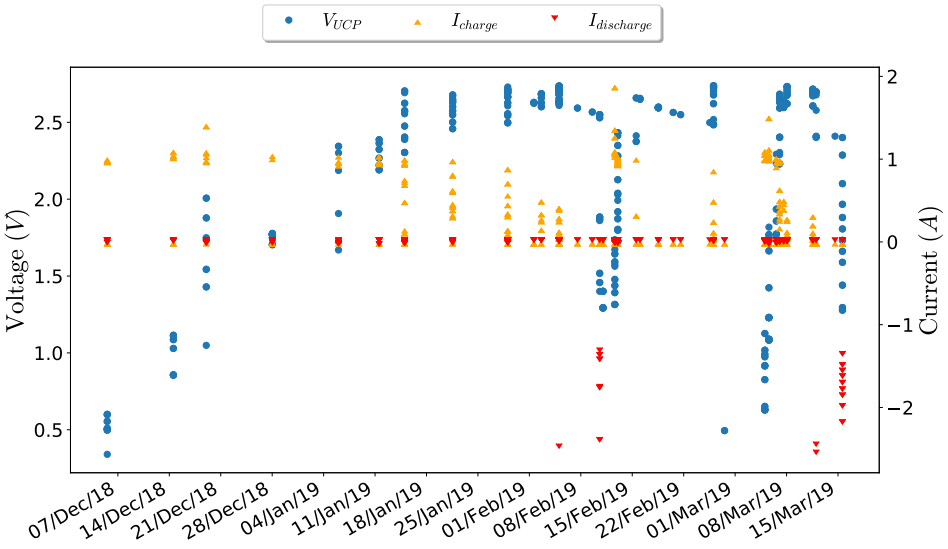

Figure 5.6: Voltage and current during charging and discharging the UCP.

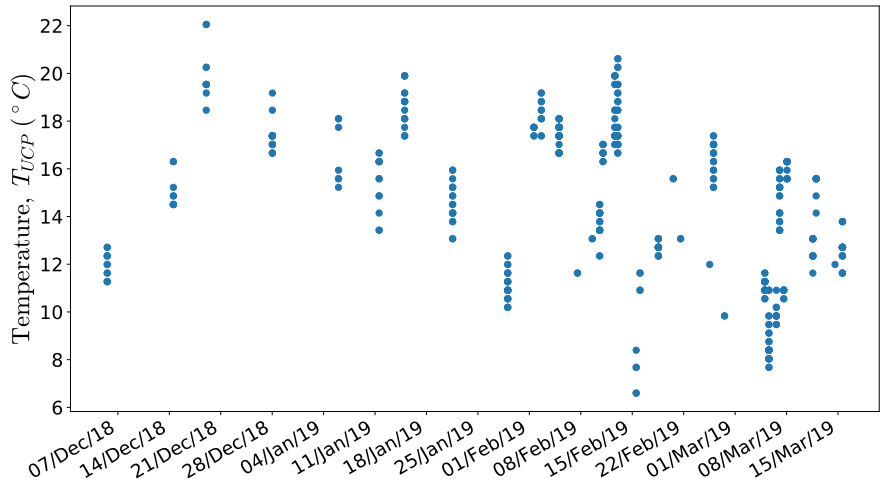

Figure 5.7: Temperature during charging and discharging the UCP.

5.3.1 Self discharge characterization

To study self-discharge in ultracapacitor in LEO, measurements were taken from orbit without charging or discharging mode. In this case, the same UCP measurements previously described were received in the Ground Station: voltage (V_{UCP}),

charge current (Ic_{UCP}), discharge current (Id_{UCP}) and temperature (T_{UCP}). Thus, the measurements used to evaluate the self-discharge of UCP meet the following two requirements: First, the time between two consecutive measurements ($dTime$) is higher that one day. Second, the current measurements are zero to assure that measurements were taken during open circuit condition. Then, the resulting measurements show the change in the voltage (dV) in the corresponding period $dTime$ (Table 5.2). The self-discharge ($selfd$) is calculated as

$$selfd = \frac{|dV|}{ucp\_v + |dV|} \tag{5.1}$$

to show the percentange of change.

Date (JST)	ucp_v (V)	ucp_T	dTime	dV (V)	dT	selfd (%)
2019-01-06 00:35:11	1.67	15.58	8 days 23:51:17	-0.10	-1.80	5.65
2019-02-02 14:58:44	2.60	17.38	1 days 00:07:37	-0.03	-0.36	0.98
2019-02-07 13:08:43	2.59	11.63	2 days 12:03:21	-0.04	-5.75	1.63
2019-02-09 13:28:02	2.57	13.07	2 days 00:19:18	-0.03	1.44	0.99
2019-02-10 13:36:13	2.55	13.43	1 days 00:08:08	-0.02	0.36	0.67
2019-02-18 13:23:12	2.60	13.07	2 days 12:01:22	-0.06	1.44	2.26
2019-02-20 13:49:14	2.56	15.58	2 days 00:20:05	-0.03	2.88	1.21
2019-02-21 13:56:32	2.55	13.07	1 days 00:07:16	-0.01	-2.52	0.56
2019-02-25 13:01:11	2.50	11.99	3 days 23:04:37	-0.05	-1.08	2.02
2019-03-14 14:18:24	2.41	11.99	2 days 13:34:26	0.00	-3.59	0.00
2019-03-15 14:29:07	2.40	12.71	1 days 00:10:43	-0.01	0.72	0.36

Table 5.2: UCP self-discharge calculation

Chapter 6

Conclusions

There is a need of improving the survival of small spacecraft due to their high failure rate. Among spacecraft subsystems, Electrical Power systems is one of the main contributors to early failure of Cubesats. Then, analysis and methods to improve the mission assurance are necessary. In this thesis, the advantages of using various configurations of power buses on small satellites to achieve minimum mission success were discussed. It is recommended to evaluate the dual-bus power architecture because it offers increased reliability at a modest increase in mass, volume and complexity, which is also proportional to development risk.

A modular approach for the power generation component of small satellites was developed. It is called Solar Module Integrated Converter. The general architecture of the SMIC, design considerations and evaluation approach were proposed and detailed. Using SMIC for solar power generation reduces the complexity in both design and testing for small satellites. This effectively reduces the development time and costs of the mission without sacrificing quality and reliability because only one module is designed and qualified. Once it is confirmed that it meets the functional requirements, as well as withstands the launch and in-orbit environments, the required number of SMIC are manufactured. In the case of Ten-Koh satellite, after one module was successfully qualified, 12 SMIC were manufactured and integrated into the spacecraft.

SMIC allows incremental development for space programs. An updated or alternative version can be designed without changing the rest of the EPS. For example, the exemplar SMIC module includes MPPT as solar array regulator for maximum power generation. Selecting DET in SMIC does not change the proposed design approach because DET also imposes restrictions on the voltage that is used as input for the solar array design. The trade-off between DET or MPPT can be challenging in certain cases and, for this reason, we limited our analysis to MPPT without loss of generality. In the same way, new SMIC can be designed changing the MPPT technique or the number of cells in the solar array to adapt the module to new missions.

Functionalities integrated into SMIC are strongly related. Solar arrays always require a solar power regulator, thus it is advantageous to have these functions in the same module. In the same way, the measurements or solar arrays are required for the housekeeping of most of the spacecraft. Thus, SMICs also contributes to the reliability of the spacecraft because they facilitate the implementation of redundancy of solar arrays, solar arrays regulator and telemetry acquisition units. In the case of Ten-Koh, 12 SMICs were connected in parallel; if one of the SMICs is damaged, then there are still 11 more providing power and their corresponding measurements.

The SMIC design for Ten-Koh followed the proposed design and qualification approach. The satellite was developed over 1.5 years and launched in October 2018, and the success of the SMIC has been confirmed via telemetry data. According to the in-orbit measurements, the total power provided by the solar array to charge the battery during sunlight was calculated to be 4–6 W. Based on this success, we are confident that the modular approach worked in Ten-Koh and the proposed method can help other missions to reduce the development time while ensuring mission success.

In brief, SMIC reduces complexity, and, hence, cost and development time. SMICs are also good because the design of the EPS is decoupled from the power source

giving the possibility to update the modules without affecting the rest of the EPS design. SMICs also facilitate the implementation of redundancy that increases the reliability of the spacecraft. However, There are some drawbacks in SMIC like the required number of harness for the telemetry acquisition unit. In addition, modularity always brings some range limitation due to the rate of the electronic devices. So, electrical interface must be clearly defined.

The results have demonstrated using a COTS ultracapacitors on board Ten-Koh for duration 5 months in orbit, the results shown clearly that the ultracapacitors kept same behavior before and after been in orbit, for charging and discharging. As future work designing hybrid system will be done based on Li-Ion and Ultracapacitors, the objective of mission will be a demonstration in orbit for almost 1 year. Other new kind of energy storage, Solid-State battery, will be demonstrated.

In addition, as future work of this thesis is proposed the following items:

- Explore the application of dual bus EPS for Cubesat platforms where power generation is limited by the available surface in the spacecraft.
- Evaluate the implementation of additional modules in EPS that can be integrated with SMIC to facilitate the EPS design. For example what would be necessary to have a module that integrates SMIC and battery cells. Thermal control and inhibits are issues that would need to be addresses.

Bibliography

[1] Kiran Kumar Pradhan. Shortening of development time of lean satellites. International Lean Satellite Workshop, Kyushu Institute of Technology, 1. Kitakyushu, Japan, 2018.

[2] Michael Swartwout and Clay Jayne. University-Class Spacecraft by the Numbers: Success, Failure, Debris. (But Mostly Success.). In *AIAA/USU Conference on Small Satellites*, 2016.

[3] Martin Langer and Jasper Bouwmeester. Reliability of CubeSats – Statistical Data, Developers' Beliefs and the Way Forward. In *AIAA/USU Conference on Small Satellites*, 2016.

[4] M N Sweeting. Modern Small Satellites-Changing the Economics of Space. *Proceedings of the IEEE*, 106(3):343–361, 2018.

[5] P. Faure, A. Tanaka, and M. Cho. Toward lean satellites reliability improvement using HORYU-IV project as case study. *Acta Astronautica*, 133:33–49, 2017.

[6] Mengu Cho, Masui Hirokazu, and Filippo Graziani. Introduction to lean satellite and ISO standard for lean satellite. In *RAST 2015 - Proceedings of 7th International Conference on Recent Advances in Space Technologies*, 2015.

[7] Mengu Cho and Filippo Graziani, editors. *Definition and Requirements of Small Satellites Seeking Low-Cost and Fast-Delivery.* International Academy of Astronautics, Paris, 2018.

[8] Jesus Gonzalez-Llorente, Alexander Lidtke, Ronald Hurtado, and Keiichi Okuyama. Single-bus and Dual-bus Architectures of Electrical Power Systems for Small Spacecraft. *Journal of Aerospace Technology and ManagementTechnology and Management*, 11, 2019.

[9] Jesus Gonzalez-Llorente, Alexander A. Lidtke, Ken Hatanaka, Ryo Kawauchi, and Kei-Ichi Okuyama. Solar Module Integrated Converters as Power Generator in Small Spacecrafts: Design and Verification Approach. *Aerospace*, 6(5):61, 2019.

[10] Valdemir Carrara, Rafael Barbosa Januzi, Daniel Hideaki Makita, Luis Felipe De Paula Santos, and Lidia Shibuya Sato. The ITASAT cubesat development and design. *Journal of Aerospace Technology and Management*, 9(2):138–147, 2017.

[11] N.H. Crisp, K. Smith, and P. Hollingsworth. Launch and deployment of distributed small satellite systems. *Acta Astronautica*, 114:65–78, 2015.

[12] Seyoung Yoon, Yuchul Shin, Jeheon Jeon, Yongmyung Seo, Jongho Jeon, Ju Woo, and Jongho Seon. Analysis of the charged particle radiation effect for a CubeSat transiting from Earth to Mars. *Current Applied Physics*, 14(4), 2014.

[13] Alessandra Babuscia, Kar-Ming Cheung, Dariush Divsalar, and Charles Lee. Development of cooperative communication techniques for a network of small satellites and CubeSats in deep space: The SOLARA/SARA test case. *Acta Astronautica*, 115:349–355, 2015.

[14] Bruno Victorino Sarli, Kaito Ariu, and Hajime Yano. PROCYON's probability analysis of accidental impact on Mars. *Advances in Space Research*, 57(9):2003–2012, 2016.

[15] Kazuya Okada, Yuki Seri, Ryunosuke Shibagaki, Hirokazu Masui, and Mengu Cho. On-orbit results of the power system on-board Nano-satellite Horyu-II. In *29th International Symposium on Space Technology and Science*, pages 1–6, Nagoya, Japan, 2013.

[16] Mohamed Yahia Edries, Atomu Tanaka, and Mengu Cho. Design and Testing of Electrical Power Subsystem of a Lean Satellite, HORYU-IV. *Transactions of The Japan Society For Aeronautical And Space Sciences, Aerospace Technology Japan*, 14(ists30):7–16, 2016.

[17] Chad Frost, Rogan Shimmin, Elwood Agasid, Roland Burton, Roberto Carlino, and Gregory Defouw. Small Spacecraft Technology State of the Art. Technical report, NASA Ames Research Center, Mission Design Division, 2015.

[18] Mukund Patel. *Spacecraft Power System*. CRC Press, Boca Raton, Florida, USA, 1st edition edition, 2005.

[19] Buck Boost Regulator (B2R) for spacecraft Solar Array Power conversion. In *Applied Power Electronics Conference and Exposition (APEC), 2010 Twenty-Fifth Annual IEEE*, pages 1313 – 1319, 2010.

[20] Didier Loche, Jean-Marc Labille, Fabrice Wallecan, and Olivier Goeij. Mono-bus and dual-bus power architecture trade-off for high power LEO Satellite. In *European Space Agency, (Special Publication) ESA SP*, 2011.

[21] Fumito Kuroiwa, Kei-chi Okuyama, Nishio Masanori, Hiroki Morita, Bianca Szasz, Sidi Bendoukha, Saganti Premkumar, and Doug Holland. A Design Method of an Autonomous Control System for a Deep-Space Probe. *Transac-*

tions of The Japan Society For Aeronautical And Space Sciences, Aerospace Technology Japan, 14(ists30):105–112, 2016.

[22] M. Hecht. Risk and Reliability. In James R. Wertz, David F. Everett, and Jeffery J. Puschell, editors, *Space Mission Engineering: The new SMAD*. Microcosm Press, Hawthorne, CA, USA, 2011.

[23] D. Del Corso, C. Passerone, L. Reyneri, C. Sansoe, S. Speretta, and M. Tranchero. Design of a university nano-satellite: The picpot case. *IEEE Transactions on Aerospace and Electronic Systems*, 47(3):1985–2007, 2011.

[24] Kei-chi Okuyama, Bianca Szasz, Bui Nam Duong, Sidi Bendoukha, Shigeru Hibino, Masanori Nishio, Saganti Premkumar, Doug Holland, and Seiji Fukushima. A System Design Method for an Ultra-Small Deep Space Probe. In *30th International Symposium on Space Technology and Science*, pages 1–7, Kobe, 2015.

[25] S. Mishra. Power supplies for consumer electronic devices. *Potentials, IEEE*, 38(1):8–13, 2019.

[26] M.H. DeGroot and M.J. Schervish. *Probability and Statistics*. Pearson Education Limited, Harlow, UK, 4th edition, 2014.

[27] Seiko Shirasaka, Yoshihiro Tsuruda, Shinichi Nakasuka, Masayasu Matsui, and Ichiro Mase. Implementation and Evaluation of Reasonably Reliable Systems Engineering. In *30th International Symposium on Space Technology and Science*, pages 1–4, 2015.

[28] J Straub and D Whalen. Student expectations from participating in a small spacecraft development program. *Aerospace*, 1(1):18–30, 2014.

[29] A. Poghosyan and A. Golkar. CubeSat evolution: Analyzing CubeSat capabilities for conducting science missions. *Progress in Aerospace Sciences*, 88:59–83, 2017.

[30] C L G Batista, A C Weller, E Martins, and F Mattiello-Francisco. Towards increasing nanosatellite subsystem robustness. *Acta Astronautica*, 156:187–196, 2019.

[31] Alessandro Menchinelli, Francesca Ingiosi, Ludovico Pamphili, Paolo Marzioli, Riccardo Patriarca, Francesco Costantino, and Fabrizio Piergentili. A Reliability Engineering Approach for Managing Risks in CubeSats. *Aerospace*, 5(4), 2018.

[32] M. Rizwan Mughal, Anwar Ali, and Leonardo M. Reyneri. Plug-and-play design approach to smart harness for modular small satellites. *Acta Astronautica*, 94(2):754–764, feb 2014.

[33] T M Lim, A M Cramer, S A Rawashdeh, and J E Lumpp. A Modular Electrical Power System Architecture for Small Spacecraft. *IEEE Transactions on Aerospace and Electronic Systems*, 54(4):1, 2018.

[34] Heesung Park. Electrical Design of a Solar Array for LEO Satellites. *International Journal of Aeronautical and Space Sciences*, 17(3):401–408, 2016.

[35] Mohammed Bekhti and M.N. Sweeting. Power system design and in orbit performance of Algeria's first micro satellite Alsat-1. *Electric Power Systems Research*, 78(7):1175–1180, jul 2008.

[36] Li Peng, Zhou Jun, and Yu Xiaozhou. Design and On-Orbit Verification of EPS for the World's First 12U Polarized Light Detection CubeSat. *International Journal of Aeronautical and Space Sciences*, 2018.

[37] A. Ali, S.A. Khan, M.A. Dildar, H. Ali, and N. Ullah. Design and thermal modeling of solar panel module with embedded reconfigurable Air-Coil for micro-satellites. *PLoS ONE*, 13(7), 2018.

[38] Edwin C.Y. Koh, Armin Förg, Matthias Kreimeyer, and Markus Lienkamp. Using engineering change forecast to prioritise component modularisation. *Research in Engineering Design*, 26(4):337–353, 2015.

[39] I. Vertat and A. Vobornik. Efficient and reliable solar panels for small CubeSat picosatellites. *International Journal of Photoenergy*, 2014, 2014.

[40] Anwar Ali, Shoaib Ahmed Khan, M. Usman Khan, Haider Ali, M. Rizwan Mughal, and Jaan Praks. Design of Modular Power Management and Attitude Control Subsystems for a Microsatellite. *International Journal of Aerospace Engineering*, 2018, 2018.

[41] Jack Claricoats, Sam M. Dakka, Jack Claricoats, and Sam M. Dakka. Design of Power, Propulsion, and Thermal Sub-Systems for a 3U CubeSat Measuring Earth's Radiation Imbalance. *Aerospace*, 5(2):63, jun 2018.

[42] Joseph K. McDermott, Jeremiah Schneider, and Scott Enger. Power. In James Wertz, David Everett, and Jeffery Puschell, editors, *Space Mission Engineering: The new SMAD*, chapter 21, pages 641–662. Microcosm press, Hawthorne, CA, USA, 2011.

[43] M M Afzal Awan and T Mahmood. A novel ten check maximum power point tracking algorithm for a standalone solar photovoltaic system. *Electronics*, 7(11), 2018.

[44] R.-M. Chao, S.-H. Ko, H.-K. Lin, and I.-K. Wang. Evaluation of a distributed photovoltaic system in grid-connected and standalone applications by different MPPT algorithms. *Energies*, 11(6):121693718, 2018.

[45] Feng Wang, Xinke Wu, F C Lee, Zijian Wang, Pengju Kong, and Fang Zhuo. Analysis of Unified Output MPPT Control in Subpanel PV Converter System. *Power Electronics, IEEE Transactions on*, 29(3):1275–1284, 2014.

[46] J. Bouwmeester, S.P. van der Linden, A. Povalac, and E.K.A. Gill. Towards an innovative electrical interface standard for PocketQubes and CubeSats. *Advances in Space Research*, 2018.

[47] R. Rocha and L. Rodrigues. Photovoltaic panels as attitude sensors for artificial satellites. *IEEE Aerospace and Electronic Systems Magazine*, 31(11):14–23, 2016.

[48] Jesus Gonzalez-Llorente, David Rodriguez-Duarte, Sergio Sanchez-Sanjuan, and Andres Rambal-Vecino. Improving the efficiency of 3U CubeSat EPS by selecting operating conditions for power converters. In *Aerospace Conference, 2015 IEEE*, pages 1–7, 2015.

[49] Spectrolab. 29.5% NeXt Triple Junction (XTJ) Solar Cells. Accessed: 2019-03-27.

[50] Azur Space. 30% Triple Junction GaAs Solar Cell Type: TJ Solar Cell 3G30C - Advanced. Accessed: 2019-03-27.

[51] CESI. Triple-Junction Solar Cell for Space Applications. Accessed: 2019-03-27.

[52] Dae Young Lee, James W. Cutler, Joe Mancewicz, and Aaron J. Ridley. Maximizing photovoltaic power generation of a space-dart configured satellite. *Acta Astronautica*, 111:283–299, jun 2015.

[53] Sergio Sanchez-Sanjuan, Jesus Gonzalez-Llorente, and Ronald Hurtado-Velasco. Comparison of the Incident Solar Energy and Battery Storage in a 3U CubeSat Satellite for Different Orientation Scenarios. *Journal of Aerospace Technology and Management*, 8(1):91–102, 2016.

[54] E. Roibás-Millán, A. Alonso-Moragón, A.G. Jiménez-Mateos, and S. Pindado. Testing solar panels for small-size satellites: The UPMSAT-2 mission. *Measurement Science and Technology*, 28(11), 2017.

[55] M.G. Villalva, J.R. Gazoli, and E.R. Filho. Comprehensive Approach to Modeling and Simulation of Photovoltaic Arrays. *IEEE Transactions on Power Electronics*, 24(5):1198–1208, may 2009.

[56] M A G de Brito, L Galotto, L P Sampaio, G de Azevedo e Melo, and C A Canesin. Evaluation of the Main MPPT Techniques for Photovoltaic Applications. *Industrial Electronics, IEEE Transactions on*, 60(3):1156–1167, 2013.

[57] S B Kjaer. Evaluation of the "Hill Climbing" and the "Incremental Conductance" Maximum Power Point Trackers for Photovoltaic Power Systems. *Energy Conversion, IEEE Transactions on*, 27(4):922–929, 2012.

[58] Z Ivanovic, B Blanusa, and M Knezic. Analytical power losses model of boost rectifier. *Power Electronics, IET*, 7(8):2093–2102, 2014.

[59] Timo Wekerle, José Bezerra Pessoa Filho, Luís Eduardo Vergueiro Loures da Costa, and Luís Gonzaga Trabasso. Status and trends of smallsats and their launch vehicles - An up-to-date review, 2017.

[60] Sidi Ahmed Bendoukha, Kei-ichi Okuyama, Szasz Bianca, and Masanori Nishio. Control System Design of an Ultra-small Deep Space Probe. *Energy Procedia*, 100:537–550, nov 2016.

[61] J. Bouwmeester and J. Guo. Survey of worldwide pico- and nanosatellite missions, distributions and subsystem technology. *Acta Astronautica*, 67(7-8):854–862, oct 2010.

[62] K.B. Chin, E.J. Brandon, R.V. Bugga, M.C. Smart, S.C. Jones, F.C. Krause, W.C. West, and G.G. Bolotin. Energy Storage Technologies for Small Satellite Applications. *Proceedings of the IEEE*, 106(3):419–428, 2018.

[63] Jesus Gonzalez-Llorente, Kei-ichi Okuyama, Isai Fajardo Tapia, Bianca Szasz, Sidi Bendoukha, and Masanori Nishio. Evaluation of Orbit data of electrical power system of deep space probe Shinen2. In *31th International Symposium on Space Technology and Science*, 2017.

[64] Andrew Burk. Ultracapacitors: why, how, and where is the technology. *Journal of power sources*, 91(1):37–50, 2000.

[65] Tatsuo Shimizu and Craig Underwood. Super-capacitor energy storage for micro-satellites: Feasibility and potential mission applications. *Acta Astronautica*, 85, 2013.

[66] Tamer Aburouk, Sangkyun Kim, Hirokazu Masui, and Mengu Cho. Design , Fabrication , and Testing of an Electrical Double-Layer Capacitor-Based 1U CubeSat Electrical Power System. *Journal of Small Satelites*, 7(1):701–717, 2018.

[67] Mihai Totu. An Innovative CubeSat Power System. *Applied Mechanics and Materials*, 436:40–46, 2013.

[68] Muhammad Alkali, Mohamed Y Edries, and Arifur R Khan. Design Considerations and Ground Testing of Electric Double-Layer Capacitors as En- ergy Storage Components for Nanosatellites. *Journal of Small Satelites*, 4(2):387–405, 2015.

[69] Keith C. Chin, Nelson W. Green, and Erik J. Brandon. Evaluation of supercapacitors for space applications under thermal vacuum conditions. *Journal of Power Sources*, 379:155–159, mar 2018.